Large-scale comparison of 3*d* and 4*d* transition metal complexes illuminates the reduced effect of exchange on second-row spin-state energetics

Aditya Nandy[1,2,#], Daniel B. K. Chu[1,#], Daniel R. Harper[1,2], Chenru Duan[1,2], Naveen Arunachalam[1], Yael Cytter[1], and Heather J. Kulik[1,*]

[1]*Department of Chemical Engineering, Massachusetts Institute of Technology, Cambridge, MA 02139*

[2]*Department of Chemistry, Massachusetts Institute of Technology, Cambridge, MA 02139*

[#]These authors contributed equally.

ABSTRACT: Density functional theory (DFT) is widely used in transition-metal chemistry, yet essential properties such as spin-state energetics in transition-metal complexes (TMCs) are well known to be sensitive to the choice of the exchange-correlation functional. Increasing the amount of exchange in a functional typically shifts the preferred ground state in first-row TMCs from low-spin to high-spin by penalizing delocalization error, but the effect on properties of second-row complexes is less well known. We compare the exchange sensitivity of adiabatic spin-splitting energies in pairs of mononuclear 3*d* and 4*d* mid-row octahedral transition metal complexes. We analyze hundreds of complexes assembled from four metals in two oxidation states with ten small monodentate ligands that span a wide range of field strengths expected to favor a variety of ground states. We observe consistently lower but proportional sensitivity to exchange fraction among 4*d* TMCs with respect to their isovalent 3*d* TMC counterparts, leading to the largest difference in sensitivities for the strongest field ligands. The combined effect of reduced exchange sensitivities and the greater low-spin bias of most 4*d* TMCs means that while over one-third of 3*d* TMCs change ground states over a modest variation (ca. 0.0–0.3) in exchange fraction, almost no 4*d* TMCs do. Differences in delocalization, as judged through changes in the metal–ligand bond lengths of spin states, do not explain the distinct behavior of 4*d* TMCs. Instead, evaluation of potential energy curves in 3*d* and 4*d* TMCs reveals that higher exchange sensitivities in 3*d* TMCs are likely due to the opposing effect of exchange on the low-spin and high-spin states, whereas the effect on both spin states is more comparable in 4*d* TMCs.

1. Introduction.

Approximate density functional theory (DFT) is widely used in studying the catalytic[1-6] and materials[7-13] properties of open-shell transition-metal complexes[14]. The well-localized *d* or *f* electrons of open-shell transition-metal centers impart unique properties but also can lead to a significant number of low-energy spin and oxidation states that are challenging to describe on equal footing using approximate electronic structure methods. For DFT in particular, presently available exchange-correlation (xc) approximations suffer from one- and many-electron self-interaction errors[15-19], commonly referred to as delocalization error[20-22] (DE).

The high earth abundance and prevalence of 3*d* transition metals in enzymatic systems has motivated the widespread study[16, 23-41] of electronic structure method accuracy in first-row transition metal complexes. For 3*d* transition-metal chemistry, DE can lead to pronounced errors in calculated bond dissociation energies[16, 23-27], barrier heights[28-29], and properties of the density[30-33] within a given spin state as well as the relative energetic ordering of spin states[29, 34-41]. While in some cases, it is possible to use higher accuracy methods such as correlated wavefunction theory, such methods have their own challenges in open-shell transition-metal complex (TMC) property prediction accuracy[42-45] and remain cost-prohibitive for large-scale discovery of new TMCs[46-51].

Although less earth abundant than 3*d* metals, 4*d* transition metals often form catalysts with superior catalytic activity and turnover number (e.g., Ru[52-54] for water oxidation and Mo[55] for hydrogen evolution) and are excellent photosensitizers[56]. Despite this importance of 4*d* transition metals, comparatively less is known about the relative accuracy of electronic structure methods for these TMCs[57-59]. While we can anticipate that there should be some transferable observations between 3*d* and 4*d* metals, a more detailed understanding of the relationship between 3*d* and 4*d* TMC sensitivity to method choice is needed.

Broadly, the need to balance cost and accuracy has motivated a number of strategies aimed at efficiently eliminating DE in approximate DFT by recovering the derivative discontinuity[60] lacking from pure (i.e., generalized gradient approximation or GGA) functionals[15, 61-66]. Approaches have included self-interaction[67-69] and closely related DFT+U[70-73] corrections, tailoring higher order terms in the xc functional[37, 40, 45, 74-85], or incorporating an admixture[32-33, 86-102] of Hartree–Fock (HF) exchange globally or with range-separation in a GGA. All such strategies generally behave similarly in TMCs by decreasing covalency[33] or dative bonding[32, 103-105] and localizing density away from the metal[30, 37]. Functional tuning for either 3*d* or 4*d* transition-metal chemistry is challenged[106] both by the limited availability of reference data and the highly system- and property-specific nature of optimal functional choice[29, 35-37, 107-112], although for select cases physically motivated tuning approaches have been developed[113-115]. Still, tuning the global amount of HF exchange (i.e., a_{HF}) in a GGA hybrid remains one of the most widely used approaches to improving approximate DFT errors.

For 3*d* midrow, octahedral TMCs, it is well known that the ground state is highly sensitive to the fraction of HF exchange due to the near-degeneracy of multiple spin states in these complexes[36, 82, 116-119] as well as the close relationship between spin-state stabilization and DEs in approximate DFT[30, 111]. Pure, semi-local GGA functionals[120-121] consistently stabilize overly-delocalized[18, 30], strongly covalent states[33], tending to favor the increased bonding in low-spin (LS) over high-spin (HS) states[29, 39, 70, 77, 122-125]. This manifestation of DE leads GGAs to predict incorrect ground states as well as relative energies[14, 124-125] between spin states (e.g., adiabatic HS to LS spin splitting, $\Delta E_{\text{H-L}}$). Hybrid functionals counteract[35-37, 118, 126-129] the bias for LS states, but the appropriate fraction of HF exchange is strongly system dependent[35-37, 108-111,

[130]. For 3*d* TMCs, conflicting proposals of low (as little as $a_{\text{HF}} = 0.0$)[35, 117, 131-132] and high ($a_{\text{HF}} = 0.4$-0.5)[31, 36, 40, 133-134] fractions have been recommended, but 4*d* TMCs do not have similar heuristics.

In this work we apply our pragmatic approach of understanding the linearized[29-31, 37, 39] exchange sensitivity on spin-splitting energies[35-37, 108, 117, 131-132] simultaneously to 3*d* and 4*d* TMC spin-state energetics. In 3*d* TMCs, this spin-state ordering exchange sensitivity is correlated to the ligand field strength of coordinating ligands[37, 108], with bare ions exhibiting reduced sensitivities[39] in comparison to strong-field ligands. For common ligands in mid-row, 3*d* TMCs, this exchange sensitivity can be significant, leading to a change in $\Delta E_{\text{H-L}}$ on the order of 10-20 kcal/mol for a change in HF exchange from $a_{\text{HF}} = 0.15$ (e.g. in B3LYP*[132]) to $a_{\text{HF}} = 0.25$ (e.g., in PBE0[135]). These strong relationships between chemical structure and method sensitivity in 3*d* TMCs have enabled the development of machine learning models to predict exchange sensitivity and exchange-dependent properties, enabling understanding of how changes in functional definition can influence large-scale discovery efforts[136-139].

Although these relationships have been established and fruitfully applied for 3*d* TMCs, the sensitivity of second-row (i.e., 4*d*) TMCs to HF exchange is not well known. In this work, we carry out a large-scale study of hundreds of mononuclear octahedral TMCs to understand broad relationships among first- and second-row spin-state ordering and exchange sensitivity. In Sec. 2, we describe how we construct a data set in which both the 3*d* and an isovalent 4*d* metal complex's properties and sensitivity to exchange are known for mid-row transition metals in low-, intermediate-, and high-spin states. In Sec. 3, we discuss our results on quantifying distinct behavior in ground state preference and sensitivity to HF exchange fraction for the second-row complexes that still maintains analogy to preferences in the first-row complexes. We identify sources for this difference by noting distinct effects of exchange on each spin state's potential energy surface in 3*d* and 4*d* TMCs. Finally, in Sec. 4, we provide our conclusions.

2. Computational details.

2a. Data set construction.

We studied the effect of HF exchange on the spin-state ordering of octahedral TMCs with a single mid-row transition-metal center. We compared properties of TMCs comprised of first-row (i.e., 3*d* valence) Cr, Mn, Fe, and Co to second-row (i.e., 4*d* valence) Mo, Tc, Ru, and Rh (Figure 1). In all cases, we calculated properties of metal centers in formal M(II) or M(III) oxidation states to ensure differences in spin state correspond to differences in *d* orbital occupations (Figure 1). The TMCs were evaluated in up to three spin states: low-spin (LS), intermediate-spin (IS), and high-spin (HS), where we defined the IS and HS states as those that differ from the LS state by two more or four more unpaired electrons, respectively. We then computed the gas phase, adiabatic spin-splitting energy: between the LS and HS states, $\Delta E_{\text{H-L}}$, as well as between the IS state and either the LS or the HS state (i.e., $\Delta E_{\text{H-I}}$ and $\Delta E_{\text{I-L}}$). The nominally d^3 Cr(III)/Mo(III) and d^7 Co(II)/Rh(II) were evaluated only in LS doublet and IS quartet spin multiplicities, and only $\Delta E_{\text{I-L}}$ was computed (Figure 1). The d^5 metals (i.e., Mn(II)/Tc(II) or Fe(III)/Ru(III)) were studied in LS doublet, IS quartet, and HS sextet states (Figure 1). Analogously, d^4 (i.e., Mn(III)/Tc(III) or Cr(II)/Mo(II)) and d^6 (i.e., Fe(II)/Ru(II) or Co(III)/Rh(III)) metals were calculated in LS singlet, IS triplet, and HS quintet states (Figure 1).

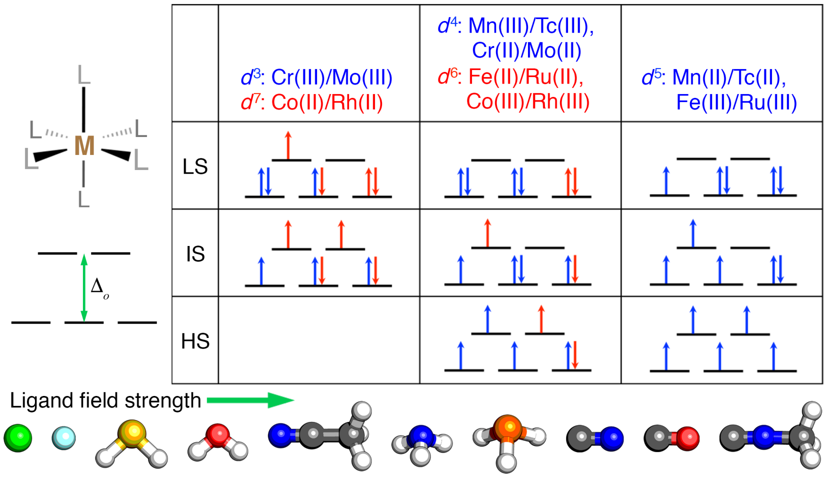

Figure 1. (top) Qualitative diagrams of electron configurations in low-spin (LS), intermediate-spin (IS), and high-spin (HS) states for the mononuclear octahedral transition-metal complexes studied in this work (schematically shown at left). For both d^3/d^7 and d^4/d^6 M(II) or M(III) complexes, the additional electrons for the later transition metal are shown in red, and the electrons that apply to both states are shown in blue. The d^3 or d^7 complexes do not have a defined HS state. (bottom) The ten main monodentate ligands studied in this work ordered by their increasing ligand field strength, which tunes the octahedral field splitting (schematically shown at left). Atoms in the ball-and-stick representation are colored as follows: H in white, C in gray, N in blue, O in red, F in light blue, P in orange, S in yellow, and Cl in green.

We calculated properties of complexes formed from combinations of ten small, monodentate ligands that spanned ligand field strengths and coordinating element identities. Negatively charged halides (Cl^- and F^-) ions are known[140] to have among the weakest field strength, while several others (i.e., phosphine, carbonyl, and cyanide) have among the highest field strengths (Figure 1). Intermediate behavior is expected of the remaining (i.e., water, ammonia, hydrogen sulfide, acetonitrile, and methyl isocyanide) ligands (Figure 1). In addition to homoleptic complexes, heteroleptic complexes were formed from up to two ligands (i.e., L_1 and L_2). Both $M(L_1)_4(L_2)_2$ TMCs with the two minority L_2 ligands either trans (i.e., aligned 180° in the TMC) or cis (i.e., 90° in the TMC) were studied along with $M(L_1)_5(L_2)$ TMCs.

2b. Electronic structure calculations.

Calculations on mononuclear, octahedral TMCs studied in this work followed an established protocol.[141-142] All initial structures were generated using molSimplify[48, 143-144], which employs OpenBabel[145-146] as a backend for ligand structure generation. These calculations were automated and checked for fidelity with molSimplify automatic design (mAD)[119, 141]. All TMCs were geometry optimized with DFT using a development version of TeraChem.[147-148] For the geometry optimizations, the standard B3LYP[149-151] global hybrid functional was employed along with modified forms in which the Hartree–Fock exchange fraction (a_{HF}) was varied from its default value of 0.20 to as low as $a_{\mathrm{HF}} = 0.00$ (i.e., a pure BLYP GGA) or as high as $a_{\mathrm{HF}} = 0.30$ in increments of 0.05 while holding the LDA/GGA exchange ratio fixed as in prior work[37, 136]. All calculations employed the LANL2DZ[152] effective core potential for transition metals and the 6-31G* basis for all other atoms. Only singlet calculations were carried out in a spin-restricted formalism, with all other spin multiplicities carried out unrestricted. Level shifting[153] was employed to aid self-consistent field (SCF) convergence with the majority spin and minority spin virtual orbitals each shifted by 0.25 Ha. Geometry optimizations were carried out in translation rotation internal coordinates[154] using the L-BFGS algorithm to default tolerances for the gradient of 4.5×10^{-4} hartree/bohr and energy difference between steps of 10^{-6} hartree.

For the mAD calculation workflow, calculations were run for 24-hour increments and resubmitted for up to five additional runs. At each resubmission, mAD applies loose geometric criteria[141] and abandons any calculations that fail these checks (ESI Table S1). In this workflow, the B3LYP ($a_{\mathrm{HF}} = 0.20$) geometry optimization was carried out first. If the B3LYP geometry optimization converged, we used the converged structure and wavefunction to initialize geometry at the adjacent increased (i.e., 0.25) or decreased (i.e., 0.15) a_{HF} values, as in prior work[136]. If these calculations converged, their structures and wavefunctions were then used for the next adjacent (e.g., increased to 0.30 or decreased to 0.10) a_{HF} value geometry optimizations. However, if an optimization failed to converge, the next a_{HF} value was not attempted.

For all converged calculations, automated data fidelity checks were employed based on refinements of prior geometric[141] and electronic structure criteria[141-142, 155] (ESI Table S1). Specifically, complexes were retained if their structure was deemed to be intact based on tighter geometric criteria than were employed during the optimization (ESI Table S2). The electronic structure criteria required that the deviation of the $\hat{S}^2$ operator from its expected value was below 1 μ_{B} and the Mulliken spin density was within 1 μ_{B} of the total spin of the molecule (ESI Table S2).

Linearized exchange sensitivities, *S*, were obtained from linear fits of the dependence of the relevant property (e.g., $\square E_{\text{H-L}}$) on a_{HF}. The resulting sensitivity (e.g., $S(\square E_{\text{H-L}})$) is reported as the change in property over the range from $a_{\text{HF}} = 0.0$ to 1.0, which we refer to as HFX as in prior work[29, 37, 136]. As long as a single, qualitatively consistent electronic state has been converged over all points, this linear approximation is known to be good for a range of properties, both energetic (e.g., spin splitting[29, 35-37, 131, 136] and reaction energies[29, 156]) and electronic[30-31, 157] in nature.

To ensure that linearized exchange sensitivities could be quantitatively obtained from collected data points, we applied a series of constraints and filtering steps. We required that at least four of seven points converged and passed data fidelity checks (ESI Table S3). We then carried out leave one out cross validation (LOOCV) of the linear fit relationship of a_{HF} with the relevant property (e.g., $\square E_{\text{H-L}}$). Individual points with LOOCV errors greater than 5 kcal/mol were removed along with any points that, upon removal, would increase the R^2 value of the remaining points to above 0.99 (ESI Table S3). If at least four points remained after this first step, the slope was evaluated between each adjacent pair of points, and these slopes were compared for changes in sign as an indication of discontinuous points that had passed the

LOOCV check. If the pair of points that changed the sign of the slope included one on the two extrema (i.e., lowest a_{HF} or highest a_{HF} value), they were removed (ESI Table S3).

For any cases that had at least four points after these two filtering steps, a best-fit line and R^2 value was computed on the remaining points (ESI Table S3). The majority (> 90%) of points after these steps had R^2 values of 0.99 or higher (ESI Table S3). To ensure fair comparison of properties of 3*d* and 4*d* TMCs, sets formed from matching pairs of ligand fields, oxidation states, and electron configurations across 3*d* and 4*d* metals were obtained. The size of this final data set was primarily limited by the smaller size of the valid 4*d* TMC dataset (ESI Table S3). All raw data, resulting R^2 values, computed sensitivities, and reasons for eliminating points or sensitivities are provided in the ESI.

Potential energy curves (PECs) of 3*d* Fe(II) and 4*d* Ru(II) in LS singlet and HS quintet states were obtained for homoleptic complexes of He atom and CO ligands also using TeraChem and B3LYP/LACVP* with modified a_{HF} values. These PECs were obtained by rigidly shifting all six He atom (CO) ligands from distances as short as 1.70 Å (1.80 Å) to as long as 2.90 Å (2.80 Å) in 0.01 Å (0.02 Å) increments, with calculations at longer bond lengths starting from the converged wavefunction at the shorter bond lengths. The He atom was selected following recent work[43] that showed it is a representative weak field ligand, and a single He atom is simpler to translate during PEC evaluation than a typical non-linear weak-field ligand (i.e., H_2O or NH_3). The CO bond length was fixed to 1.125 Å, its value in relaxed TMCs. These calculations were repeated for a_{HF} fractions increasing from 0.0 to 0.45 in increments of 0.05, with wavefunctions always initializing from shorter bond lengths and lower a_{HF} values. All total energies and computed sensitivities are provided in the ESI.

3. Results and discussion.

3a. Ligand field sensitivity trends in homoleptic TMCs.

To understand the extent to which previous observations[35-38, 40, 126, 131] in first-row transition metals are likely to be generalizable to the second row, we first compared spin-splitting properties for a subset of homoleptic complexes. Depending on the field strength of the ligand, 3*d* Fe(II) TMCs are known to favor distinct ground states[140]. For example, d^6 Fe(II) TMCs with intermediate-field nitrogen-coordinating ligands commonly exhibit spin crossover (SCO)[158] phenomena by changing from an LS singlet to HS quintet state with increasing temperature. The $\Delta E_{\text{H-L}}$ for these complexes is sensitive to HF exchange fraction, becoming more negative with increasing a_{HF}. The combination of this physical phenomenon with sensitivity to DFT functional parameters means that different a_{HF} values can predict the same complex to have either an LS or HS ground state[35-38, 40, 126, 131].

Indeed, for the complexes studied in this work, homoleptic complexes of Fe(II) with acetonitrile or cyanide have near-degenerate LS and HS states when evaluated with B3LYP and thus are predicted to be LS with lower HF exchange (i.e., $a_{\text{HF}} = 0.1$) but HS with higher fractions (i.e., $a_{\text{HF}} = 0.3$, Figure 2). Consistent with prior observations[36-37, 136], the magnitude of this typically negative exchange sensitivity, *S*, generally increases with field strength. This means that a hexa-carbonyl Fe(II) complex that is strongly LS with B3LYP can become HS with higher exchange fractions (ca. $a_{\text{HF}} = 0.4$), whereas weak-field hexa-aqua Fe(II) is uniformly HS for all a_{HF} values (Figure 2).

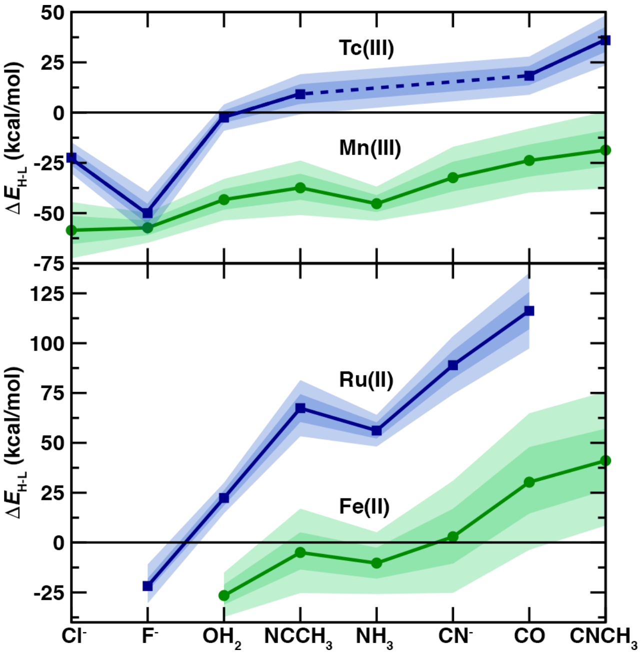

Figure 2. The HS-LS adiabatic spin splitting ($\Delta E_{\text{H-L}}$, in kcal/mol) for isovalent 3*d* (in green) and 4*d* (in blue) homoleptic TMCs: Tc(III) and Mn(III) (top) or Fe(II) and Ru(II) (bottom). Ligands have been ordered on the x-axis roughly according to ligand field strength with the metal-coordinating atom listed first in the chemical name. The points (circles for 3*d*, squares for 4*d*) correspond to values at a_{HF} = 0.2, the inner translucent shaded regions correspond to the a_{HF} = 0.1–0.3 range, and the outer translucent shaded regions correspond to a_{HF} = 0.0–0.4. A zero axis is shown to indicate where spin state ordering changes between HS and LS states. A dashed line for Tc(III) indicates that no data is available for NH_3 and CN^- complexes.

In comparison to their first-row counterparts, the isovalent 4*d* Ru(II) TMCs are considerably low-spin shifted, with almost all Ru(II) complexes strongly favoring LS states over HS states except for the weakest field (i.e., hexa-fluoride) cases (Figure 2). The Ru(II) homoleptic complexes also exhibit uniformly reduced exchange sensitivities (Figure 2). Thus, complexes with modest B3LYP $\Delta E_{\text{H-L}}$ values (e.g., hexa-aqua Ru(II), ca. 25 kcal/mol) are not predicted to change their ground state with varied a_{HF} in contrast to Fe(II) homoleptic complexes (Figure 2). Despite these differences, qualitative trends with ligand field strength appear preserved from Fe(II) to Ru(II), with increasing exchange sensitivity apparent with increasing ligand field (Figure 2).

Given the strong LS shift of 4*d* Ru(II) TMCs with respect to their 3*d* Fe(II) TMC counterparts, we identified d^4 Tc(III) as a possible metal/oxidation state where TMCs could be expected to favor HS or LS states depending on field strength (Figure 2). The 4*d* Tc(III) singlet LS and quintet HS states are in fact close in energy with B3LYP for weak-field (i.e., hexa-aqua) and intermediate-field (i.e., hexa-acetonitrile) complexes (Figure 2). The isovalent Mn(III) complexes are comparatively HS shifted, with only the homoleptic methyl-isocyanide (misc) with a pure BLYP (i.e., $a_{\text{HF}} = 0.0$) GGA coming close to spanning the LS–HS transition (Figure 2). The exchange sensitivity of all Mn(III) homoleptic TMCs is reduced with respect to the Fe(II) TMCs but follows a consistent trend of increasing with increasing ligand field strength (Figure 2). Consistent with 3*d*/4*d* observations from Fe(II)/Ru(II), Tc(III) homoleptic TMCs have reduced exchange sensitivity compared to isovalent Mn(III) (Figure 2). This means that even though a number of 4*d* Tc(III) TMCs have modest B3LYP $\Delta E_{\text{H-L}}$ (< 25 kcal/mol) values, the only ground state assignment change for Tc(III) in this series would be for the B3LYP HS hexa-aqua complex to become LS with a_{HF} reduced to 0.1 or below (Figure 2). Overall, reduced exchange sensitivities in these 4*d* TMCs (i.e., whether with Ru(II) or Tc(III)) would require the B3LYP $\Delta E_{\text{H-L}}$ to be within ±10 kcal/mol as opposed to ±25 kcal/mol for comparable 3*d* TMCs for the 4*d* TMC spin-state preference to change with HF exchange.

Both d^6 Fe(II)/Ru(II) and d^4 Mn(III)/Tc(III) TMCs have an IS triplet state. We thus also calculated the IS state to obtain $\Delta E_{\text{H-I}}$ and $\Delta E_{\text{I-L}}$ as well as their sensitivities (i.e., $S(\Delta E_{\text{H-I}})$ and $S(\Delta E_{\text{I-L}})$) for select homoleptic TMCs. We selected hexa-carbonyl TMCs as representative strong-field complexes and hexa-aqua as representative weak-field complexes (Figure 3). All 4*d* TMCs favor IS states over HS states with B3LYP (i.e., $\Delta E_{\text{H-I}} > 0$) unlike the isovalent 3*d* TMCs (Figure 3). Spin-state orderings change with a_{HF} due to high *S* for several of the 3*d* TMCs (i.e., HS-IS/HS-LS Fe(II)(CO)$_6$, IS-LS Fe(II)(H$_2$O)$_6$, and HS-IS Mn(III)(CO)$_6$) but only one of the 4*d*

TMCs (i.e., HS-LS Tc(III)(H_2O)$_6$) in part due to the reduced exchange sensitivity of 4*d* TMCs (Figure 3).

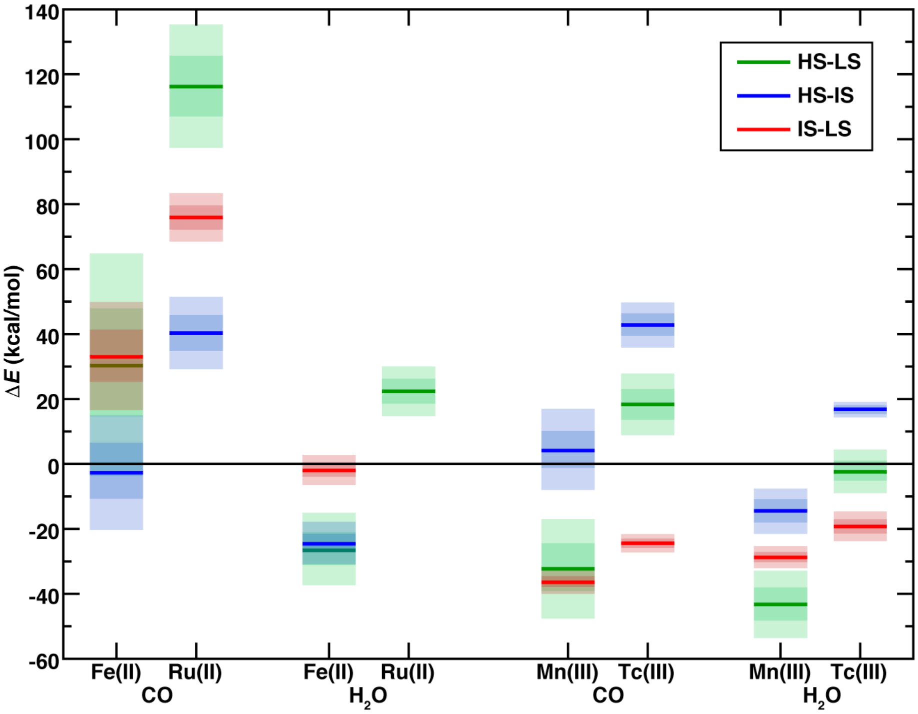

Figure 3. Comparisons of adiabatic spin splitting (Δ*E*, in kcal/mol) for HS-LS (green lines and shading), HS-IS (blue lines and shading) and IS-LS (red lines and shading) for pairs of homoleptic TMCs grouped first by the isovalent 3*d* and 4*d* metals (i.e., Fe(II)/Ru(II) vs Mn(III)/Tc(III)) and then by ligand (i.e., CO vs H_2O), as indicated on the *x*-axis. The solid lines correspond to values at a_{HF} = 0.2, the inner translucent shaded regions correspond to the a_{HF} = 0.1–0.3 range, and the outer translucent shaded regions correspond to a_{HF} = 0.0–0.4. A zero axis is shown to indicate where ordering changes for any pair of states. The Ru(II)(H_2O)$_6$ IS state was eliminated during filtering steps, and so its HS-IS or IS-LS data is unavailable.

For all spin-splitting energies, the hexa-aqua exchange sensitivities are lower than those for hexa-carbonyl in both 3*d* and 4*d* TMCs (Figure 3). As can be expected[39-40], $S(\Delta E_{\mathrm{H\text{-}I}})$ and $S(\Delta E_{\mathrm{I\text{-}L}})$ are reduced with respect to $S(\Delta E_{\mathrm{H\text{-}L}})$, with $S(\Delta E_{\mathrm{I\text{-}L}})$ consistently the uniformly smallest of the three (Figure 3). The trend holds across the over 150 pairs of 3*d*/4*d* heteroleptic or homoleptic TMCs for which all three spin-state energies have been evaluated. On average, $S(\Delta E_{\mathrm{I\text{-}L}})$ and $S(\Delta E_{\mathrm{H\text{-}I}})$ values are 38% and 62% of $S(\Delta E_{\mathrm{H\text{-}L}})$, respectively (ESI Table S4). That is, when the 4*d* TMC *S* value is reduced with respect to its 3*d* TMC counterpart, this reduction is proportional across both spin states and ligand chemistry.

3b. Global comparison of 3*d* and 4*d* TMCs.

We next expanded our comparison of HS-LS energies and their sensitivities to include heteroleptic complexes for an overall set of more than 200 d^4-d^6 TMC pairs. Over all of these 3*d*/4*d* TMC pairs, the 4*d* $S(\Delta E_{\text{H-L}})$ was consistently reduced with respect to that for 3*d* TMCs (Figure 4). The largest (i.e., most negative) 3*d* $S(\Delta E_{\text{H-L}})$ values are larger than those of 4*d* TMCs by around 50 kcal/mol·HFX (i.e., around 40% larger, ESI Table S5). For each 3*d* metal/oxidation state, average exchange sensitivities also vary, i.e., highest for Mn(II) or Fe(II) and lowest for Cr(II), with similar trends for the isovalent 4*d* metal/oxidation states (ESI Table S5). The overall reduced sensitivities of 4*d* TMCs become more apparent the larger the 3*d* TMC *S* values are (Figure 4). Based on prior analysis[36-37, 136] and our observations on homoleptics, this should mean that strong-field 3*d* TMCs are much more sensitive to HF exchange than 4*d* TMCs while weak-field 3*d* and 4*d* TMCs complexes have more similar exchange sensitivity (Figure 4). Indeed, the sensitivities of the prototypical strong-field hexa-carbonyl and weak-field hexa-aqua homoleptics largely reside at extremes of the overall relationship between 3*d* and 4*d* TMC *S* values (Figure 4).

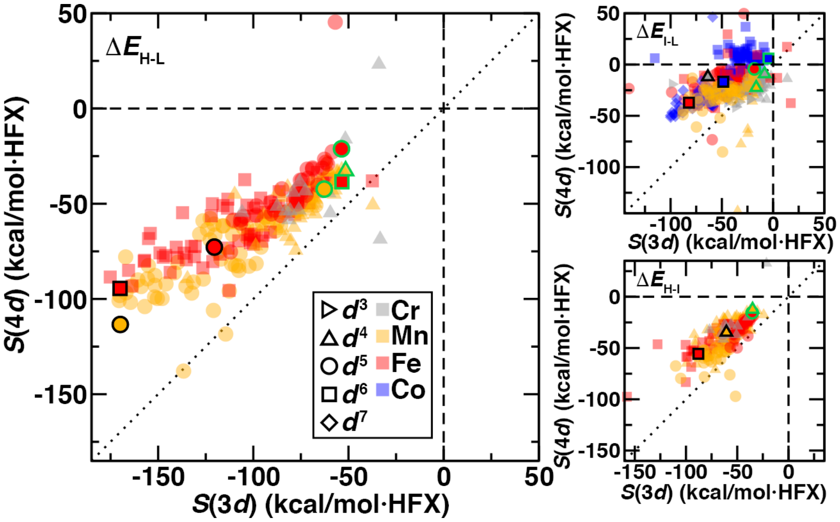

Figure 4. Sensitivities, *S*, of 3*d* vs 4*d* ligand-matched TMCs (in kcal/mol·HFX) for $\Delta E_{\text{H-L}}$ (left), $\Delta E_{\text{I-L}}$ (top, right), and $\Delta E_{\text{H-I}}$ (bottom, right). Translucent symbols are colored by element: Cr in gray, Mn in orange, Fe in red, and Co in blue. The formal electron configuration of each point is indicated by the symbol shape: d^3 right-pointing triangles, d^4 up-pointing triangles, d^5 circles, d^6 squares, and d^7 diamonds. The d^3 and d^7 data is only available for $\Delta E_{\text{I-L}}$. All hexa-aqua complexes are filled solid and outlined in green, and all hexa-carbonyl complexes are filled solid and outlined in black. The zero axis for both sensitivities is shown as a dashed black line, and a black dotted parity line is also shown.

There are a few noteworthy exceptions where the 4*d* TMC *S* exceeds that of its 3*d* TMC counterpart, namely: i) in weak-field, hexafluoro complexes of Mn(III)/Tc(III) (*S*(3*d*) ca. -35 vs *S*(4*d*) -50 to -70 kcal/mol·HFX) and ii) in stronger fields (e.g., Mn(II)$(NCCH_3)_4(CNCH_3)_2$) where the 3*d* TMC sensitivity is typical but the Tc(II) value is among the largest evaluated for 4*d* TMCs (ESI Table S6). The strong net negative charge on the halide complexes also results in other types of outliers: Ru(III) hexafluoride and a Cl^--containing Mo(II) complex are the only two 4*d* TMC cases for which the *S*($\Delta E_{\text{H-L}}$) is weakly (ca. 20-45 kcal/mol·HFX) positive (ESI Table S7). In both 4*d* TMCs, the corresponding 3*d* TMC still has a negative, albeit small *S* (ESI Table S7).

Trends for the 2-electron $\Delta E_{\text{H-I}}$ are largely consistent with those for the 4-electron $\Delta E_{\text{H-L}}$. Although overall *S*($\Delta E_{\text{H-I}}$) values for both 3*d* and 4*d* TMCs are lower than *S*($\Delta E_{\text{H-L}}$), 3*d* TMC sensitivities nearly always exceed their 4*d* TMC values (Figure 4 and ESI Table S5). The 3*d*/4*d* metal/oxidation states with the highest average *S*($\Delta E_{\text{H-L}}$) (i.e., Mn(II)/Tc(II) and Fe(II)/Ru(II)) also have the highest *S*($\Delta E_{\text{H-I}}$) values (ESI Table S5). On average, best-fit lines relating *S*(4*d*) vs *S*(3*d*) for $\Delta E_{\text{H-L}}$ and $\Delta E_{\text{H-I}}$ have comparable ratios of change in *S*(4*d*) per change in *S*(3*d*) of 0.55 and 0.65, respectively (ESI Table S5). As in the case of $\Delta E_{\text{H-L}}$, a small number of 4*d* TMC $\Delta E_{\text{H-I}}$ sensitivities exceed their 3*d* TMC counterparts and typically correspond to Mn(II) complexes with strong-field equatorial ligands (CO or $NCCH_3$) expected to have strong Jahn–Teller distortion (ESI Table S6).

We also analyzed 2-electron $\Delta E_{\text{I-L}}$ pair trends, which additionally include d^3 Cr(III)/Mo(III) and d^7 Co(II)/Rh(II) TMCs (see Figure 1). As in the other two cases of spin-splitting energetics, 4*d* TMCs exhibit reduced exchange sensitivity with respect to 3*d* TMCs (Figure 4 and ESI Table S5). For the metal/oxidation states for which only $\Delta E_{\text{I-L}}$ is defined, *S*(4*d*):*S*(3*d*) ratios from best-fit lines of 0.42 for d^3 and 0.64 for d^7 are comparable to the values of *S* observed for d^4/d^6 TMCs in all spin states (ESI Table S5). Several more 4*d* TMC outliers that are close to parity are observed, typically Mn(III)/Tc(III) complexes with equatorial chlorides or Cr(II)/Mo(II) complexes with equatorial ammonia ligands (Figure 4 and ESI Table S6). Far more positive 4*d* TMC sensitivities are observed for several Rh(III) complexes with a range of weak- and strong-field ligands (ESI Table S8). A handful of 3*d* TMCs (e.g., in Fe(II) complexes with CN^- ligands) also have positive sensitivities, but the equivalent, isovalent Ru(II) TMCs have weakly negative sensitivities (ESI Table S8). These observations on $\Delta E_{\text{I-L}}$ are distinct from $\Delta E_{\text{H-L}}$ and $\Delta E_{\text{H-I}}$ where only one cis $Mo(II)(NH_3)_4(Cl^-)_2$ complex had positive 4*d* TMC sensitivities for both quantities (ESI Table S7).

3c. Analysis of a heteroleptic complex series.

Given the diversity of TMC chemistry in these larger data sets, we simplified our analysis to understand the extent to which trends in ΔE and $S(\Delta E)$ were additive in a narrower subset of representative 3*d* and 4*d* TMC complexes. To assess the additive nature of ligand contributions, we chose a subset of the data consisting of homoleptic complexes of a weak-field ligand (H_2O), the homoleptic complexes of a strong-field ligand (CO), and the heteroleptic complexes with both ligands present. In addition to their differing field strengths, H_2O and CO were chosen for their neutral charge, eliminating the need to compare TMCs of differing net charge. For a fixed metal, oxidation state, and principal quantum number, the full set can contain up to six mixed

H_2O/CO complexes between the homoleptic hexa-aqua and hexa-carbonyl limits. This includes two cases where a single ligand of the minority type is in the complex (i.e., 5+1: $(CO)_5(H_2O)$ or $(H_2O)_5(CO)$) as well as four cases where two ligands of the alternate type are included in either a cis (i.e., equatorial/axial adjacent) or trans (i.e., axial) conformation (e.g., $(CO)_4(H_2O)_2$ or $(H_2O)_4(CO)_2$). Although the exchange sensitivity of homoleptic 3*d* TMCs has been widely studied[35-37, 118, 126-129], the expected exchange sensitivity of this type of heteroleptic TMCs is not well established for either 3*d* or 4*d* TMCs.

There is a smooth, nearly monotonic increase in $\square E_{\text{H-L}}$ with increasing number of strong-field CO ligands for Fe(II) or Ru(II) complexes (Figure 5). For the Fe(II) TMCs, B3LYP LS states become stabilized over HS states for four or more CO ligands, whereas all Ru(II) complexes are uniformly LS (Figure 5). The trend of increasing $\square E_{\text{H-L}}$ with increasing CO number is largely consistent between Ru(II) and Fe(II), but B3LYP $\square E_{\text{H-L}}$ for Ru(II) is more sensitive to the number of CO ligands (Figure 5). Interestingly, the only exception to the monotonic trend is the trans $(H_2O)_4(CO)_2$ isomer, with an $\square E_{\text{H-L}}$ closer to that for the mono-carbonyl complexes (Figure 5 and ESI Tables S9–S10). The cis $(H_2O)_2(CO)_4$ isomer has been filtered from the dataset, prohibiting broader conclusions about cis/trans isomers (see ESI data). For the Fe(II) TMCs, all mixed H_2O/CO complexes span the LS/HS transition between $a_{\text{HF}} = 0.0$ and 0.4 (Figure 5). While Fe(II) TMC S values are significantly larger than for Ru(II) TMCs, both 3*d* and 4*d* complexes appear to have a monotonic increase in sensitivity with the addition of more strong field ligands (Figure 5 and ESI Table S11).

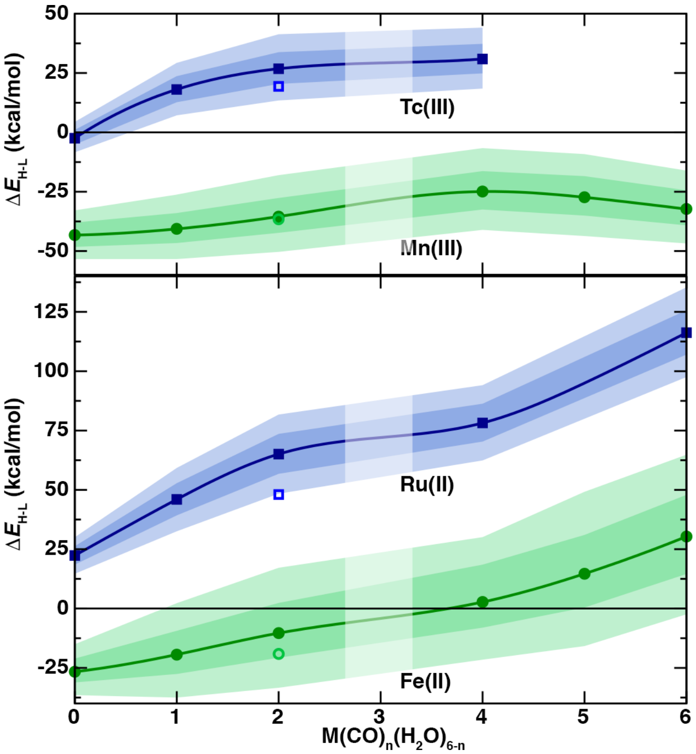

Figure 5. Properties of complexes formed by mixing H_2O and CO ligands. Variation of 4-electron $\Delta E_{\text{H-L}}$ (in kcal/mol) with increasing number of CO ligands for isovalent Mn(III)/Tc(III) or Fe(II)/Ru(II). The points (circles for 3*d*, squares for 4*d*) correspond to values at $a_{\text{HF}} = 0.2$, the inner translucent shaded regions correspond to the $a_{\text{HF}} = 0.1$–0.3 range, and the outer translucent shaded regions correspond to $a_{\text{HF}} = 0.0$–0.4. A zero axis is shown to indicate where spin-state ordering changes. A spline has been fit through the $a_{\text{HF}} = 0.2$ values excluding the open, lighter colored symbol, which corresponds to an outlier trans configuration with two CO ligands. No cis data is available for the case with four CO ligands, and no calculations were attempted for 3 CO ligands, as indicated by vertical translucent bar.

For the series of d^4 Mn(III)/Tc(III) TMCs, reduced overall ligand field dependence of both $\Delta E_{\text{H-L}}$ and *S* is observed with respect to Fe(II)/Ru(II) TMCs (Figure 5 and ESI Tables S9 and S11). The 3*d* Mn(III) TMCs are uniformly HS-favored regardless of a_{HF} value (Figure 5). Both $\Delta E_{\text{H-L}}$ and *S* values appear to reach a maximum for Mn(III) complexes once all four equatorial ligands are CO with no effect of added CO axial ligands (Figure 5). This likely occurs both because of the reduced ligand-field sensitivity of Mn(III) and non-monotonic geometric changes for the most CO-saturated Mn(III) complexes (see ESI data). Overall trends are consistent between Tc(III) and Mn(III), although the 4*d* TMC is again marked by reduced *S* values with respect to the isovalent 3*d* TMCs (Figure 5). Given the reduced sensitivities of 4*d* TMCs, only the homoleptic aqua Tc(III) complex spans the LS-to-HS transition, whereas even the modest $\Delta E_{\text{H-L}}$ (< 15 kcal/mol) in the mono-carbonyl Tc(III) complex remains LS-favored over all a_{HF} values (Figure 5).

We performed a similar analysis of the d^5 Fe(III)/Ru(III) and Mn(II)/Tc(II) metal/oxidation state pairs for which multiple CO/H_2O complex $S(\Delta E_{\text{H-L}})$ values were computed (ESI Table S11). Across the series of TMCs for this expanded set of metals, addition of strong-field carbonyl ligands has a largely monotonic, linearly increasing effect on *S* values starting from the lower extreme of homoleptic hexa-aqua TMCs and moving toward the upper extreme of hexa-carbonyl TMCs (Figure 6 and ESI Table S11). Over this set, the most significant deviations in *S* between 3*d*/4*d* TMC pairs occurs for the Fe(II)/Ru(II) cases (i.e., up to a 60 kcal/mol·HFX difference) but remains substantial for most metals, excluding only the Mn(III)/Tc(III) pairs which have somewhat reduced overall *S* values (Figure 6). The cis $(H_2O)_4(CO)_2$ complexes have significantly higher sensitivities for both 3*d* and 4*d* metals than their trans counterparts, with the exception of Mn(III)/Tc(III) (Figure 6).

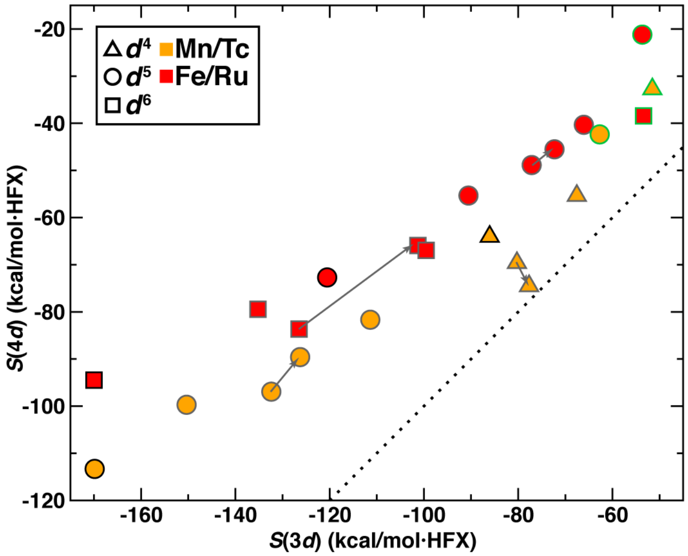

Figure 6. Properties of complexes formed by mixing H_2O and CO ligands. $S(3d)$ vs $S(4d)$ for $\Delta E_{\text{H-L}}$ (in kcal/mol·HFX) of Mn/Tc and Fe/Ru TMCs with CO or H_2O ligands in both oxidation states, colored by element (Mn/Tc in orange or Fe/Ru in red) and with symbols corresponding to formal electron configuration (d^4 in up triangles, d^5 in circles, and d^6 in squares). All hexa-aqua complexes are outlined in green, all hexa-carbonyl complexes are outlined in black, and the remaining symbols are outlined in dark gray. A gray arrow shows the path from each cis to trans $(H_2O)_4(CO)_2$ sensitivity. A dotted parity line is shown for reference.

We next compared trends in this ligand series for ΔE and $S(\Delta E)$ in the case of the 2-electron HS-IS and IS-LS spin state splitting. For $\Delta E_{\text{H-I}}$, increasing the number of CO ligands shifts the B3LYP preference from HS to IS for most 3*d* metals (i.e., excluding only Mn(III) and Fe(II)), but the 4*d* TMC preference remains uniformly IS regardless of complex composition (ESI Tables S12 and S13). Although $S(\Delta E_{\text{H-I}})$ is lower than $S(\Delta E_{\text{H-L}})$, the 3*d* TMC spin-state preference can still shift depending upon a_{HF} value (e.g., trans Fe(II)$(H_2O)_4(CO)_2$ is IS-favoring for $a_{\text{HF}} = 0.15$ but HS for B3LYP, ESI Table S12). The relationships of 3*d* and 4*d* TMC $S(\Delta E_{\text{H-I}})$ values are similar to that for $S(\Delta E_{\text{H-L}})$: i) the smallest to largest *S* magnitudes are typically bounded by the homoleptic hexa-aqua and hexa-carbonyl complexes, respectively, and ii) mixed complexes with more CO ligands have larger sensitivities especially in 3*d* versus 4*d* TMCs (ESI Figure S1 and Table S14).

For $\Delta E_{\text{I-L}}$, multiple d^3 Cr(III)/Mo(III) and d^7 Co(II)/Rh(II) complexes could also be compared (ESI Tables S15 and S16). Reduced exchange sensitivity for IS-LS pairs mean that few ground state assignments change in either 3*d* or 4*d* TMCs with change in functional (ESI Table S14). Across all metals, the trend of increasing deviation of 3*d* and 4*d* *S* values with increasing ligand field strength is preserved, consistent with HS-LS and HS-IS behavior for mixed-ligand complexes (ESI Figure S2). Nevertheless, early d^3 Cr(III)/Mo(III) and d^4 Mn(III)/Tc(III) complexes all have comparable, modest exchange sensitivities (ESI Figure S2). While most hexa-aqua complexes have the smallest sensitivities, non-monotonic behavior with number of CO ligands is observed for the IS-LS sensitivities, and several of the Rh(III) complexes have positive $S(\Delta E_{\text{I-L}})$ sensitivities (ESI Figure S2). As a possible explanation for the distinct behavior of IS-LS spin splitting trends among complexes, we considered differences in closed shell LS states (i.e., for d^4 and d^6) and open shell ones (i.e., for d^5) but observe no difference in trends (ESI Figure S2). The greater variability is likely due to noise in evaluating the lower IS-LS S values, in line with prior observations[29, 136], and the larger range of metals and oxidation states. Despite some differences for IS-LS in comparison to HS-IS or HS-LS spin-splitting energies, the ligand series analysis suggests overall that there are consistently greater differences in the effect of exchange on 3*d* than 4*d* TMCs that grow with ligand field strength.

3d. Effect of exchange on spin-state ordering.

TMC spin-state splitting sensitivities depend both on row (3*d* vs 4*d*) and electron configuration (eg., d^4 vs d^6) of the metal atom and on the strength of the ligand field. The combined effect of these differences can be further understood by evaluating how the distribution of $\Delta E_{\text{H-L}}$ shifts with HF exchange fraction. For this comparison, we chose 64 Fe(II)/Ru(II) and 51 Tc(III)/Mn(III) metal/oxidation state pairs where 3*d* TMCs and 4*d* TMCs span the HS–LS transition, respectively (Figure 7). For Fe(II) TMCs, increasing HF exchange from a pure GGA to 30% has a strong effect on the distribution of $\Delta E_{\text{H-L}}$ values (Figure 7). Because complexes with strong-field ligands have more negative sensitivities than complexes with weak field ligands, the width of the Fe(II) $\Delta E_{\text{H-L}}$ distribution decreases monotonically from $a_{\text{HF}} = 0.0$ (-75 to 80 kcal/mol) to $a_{\text{HF}} = 0.3$ (-90 to 30 kcal/mol, Figure 7). We note that a complex with $|\Delta E_{\text{H-L}}| \leq 5$ kcal/mol could be a spin crossover (SCO) complex. Using this definition, the number of potential Fe(II) SCOs is maximal for moderate, $a_{\text{HF}} = 0.1$–0.2 exchange but decreases again at higher exchange values (Figure 7). From $a_{\text{HF}} = 0.0$ to 0.30, the population of HS-favored Fe(II) TMCs also increases dramatically from 12 to 49 of 64 complexes (Figure 7 and ESI Table S17).

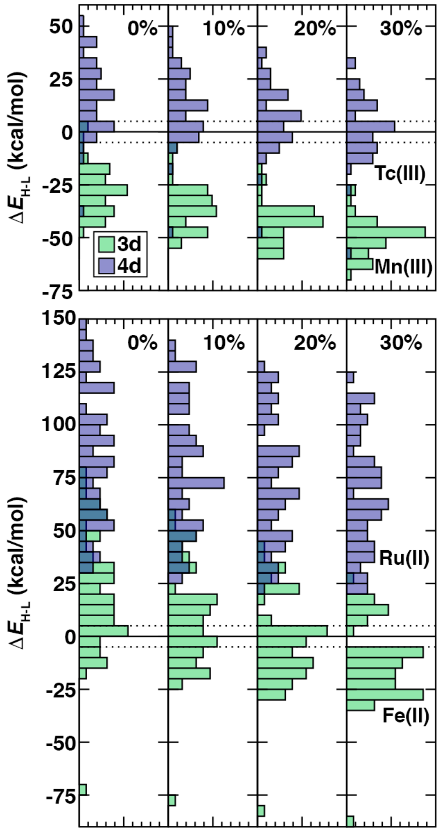

Figure 7. Normalized histograms of □$E_{\text{H-L}}$ (in kcal/mol) (bin width: 5 kcal/mol) for 51 pairs of 3*d* Mn(III) and 4*d* Tc(III) TMCs (top) and 64 pairs of 3*d* Fe(II) and 4*d* Ru(II) TMCs (bottom). Histograms are filled translucent for 3*d* (green) and 4*d* (dark blue) TMCs to show regions of overlap. A zero line is indicated as black solid where HS-LS spin state ordering changes, and a range of 5 kcal/mol around that line is indicated with black dotted lines. The panes correspond to increasing % HF exchange from left to right, as labeled in top inset.

The isovalent Ru(II) TMCs span nearly as wide a range for a_{HF} = 0.0 (30 to 150 kcal/mol) as the 3*d* TMCs, but none are HS at any exchange fraction (Figure 7 and ESI Table S17). Modest differences in exchange sensitivity across Ru(II) complexes have a limited effect on the shape of the distribution in comparison to Fe(II) TMCs (Figure 7). The range of the Ru(II) □$E_{\text{H-L}}$ distribution for a_{HF} = 0.3 (20 to 125 kcal/mol) is reduced, but this reduction (12%) is smaller than was observed for the Fe(II) TMCs (19%).

For the Tc(III)/Mn(III) isovalent pairs, the 4*d* TMCs have a more even distribution of HS and LS ground states (Figure 7). This is particularly true (18 LS and 33 HS) at $a_{\text{HF}} = 0.30$, while LS is generally favored by Tc(III) TMCs (44 LS and 7 HS) at $a_{\text{HF}} = 0.0$, and all a_{HF} values have a significant number of potential Tc(III) HS-LS SCOs (Figure 7 and ESI Table S17). In contrast to Fe(II), most (49 of 51) Mn(III) TMCs are HS even for $a_{\text{HF}} = 0.0$, and all are significantly HS (i.e., outside of the SCO region) for $a_{\text{HF}} = 0.1$ and higher (Figure 7 and ESI Table S17). The Mn(III) $\Delta E_{\text{H-L}}$ values span a smaller range than the Fe(II) TMCs, meaning that even though the width of the Mn(III) $\Delta E_{\text{H-L}}$ distribution narrows only slightly with increasing HF exchange ($a_{\text{HF}} = 0.0$: -50 to 5 kcal/mol vs $a_{\text{HF}} = 0.3$: -25 to -70 kcal/mol), this 18% reduction is roughly comparable to that for Fe(II) (Figure 7). For the Tc(III) $\Delta E_{\text{H-L}}$ distribution, there is no change in the width due to sensitivities of outliers in the distribution tails (Figure 7). Nevertheless, both Tc(III) and Mn(III) distributions become more peaked at intermediate values of the $\Delta E_{\text{H-L}}$ range, and the effect of a_{HF} on the shape of both distributions is more modest than for Fe(II) but more significant than for Ru(II) TMCs (Figure 7).

Over all 3*d*/4*d* metal/oxidation state pairs for which $\Delta E_{\text{H-L}}$ was calculated, trends are similar to those observed for Fe(II)/Ru(II) and Tc(III)/Mn(III) (ESI Table S17). The HS-LS preference of 3*d* TMCs is highly sensitive to exchange, with an even number of LS-favoring vs HS-favoring 3*d* TMCs at $a_{\text{HF}} = 0.0$ becoming predominantly (90%) HS at $a_{\text{HF}} = 0.3$ or higher (ESI Table S17). The 4*d* TMCs almost exclusively favor LS states at $a_{\text{HF}} = 0.0$, and a much smaller number (i.e., 28) of TMCs, typically with Tc(III) and to a lesser extent Tc(II) or Mo(II), becoming HS-favored at $a_{\text{HF}} = 0.3$ (ESI Table S17). Thus, based on this analysis, the 4*d* TMC LS-bias with respect to 3*d* TMCs combined with reduced exchange sensitivity also makes the 4*d* TMC HS/LS preferences significantly less sensitive to a_{HF} values.

Ultimately, to quantify the effect of HF exchange on 3*d*/4*d* TMC ground state (GS) assignment, we extended the comparison of spin-state energetics to include IS states. There are 155 d^4-d^6 3*d*/4*d* TMC pairs for which all three (i.e., HS, IS, and LS) spin states and the spin-splitting energy sensitivities are computed. We combine these pairs with the 92 d^3 or d^7 3*d*/4*d* TMC pairs for which only two states were accessible (i.e., IS and LS), and their energies were computed. Over this 247 complex set, significant differences in the sensitivity of GS assignment to a_{HF} are apparent between 3*d* and 4*d* TMCs (Figure 8). Namely, the number of HS ground states rises from around one in five at a_{HF} = 0.0 to over half at a_{HF} = 0.3 for 3*d* TMCs, whereas none of the 4*d* TMCs have a HS GS at any a_{HF} value (Figure 8 and ESI Tables S18–S19). The proportion of IS states remains roughly constant for 3*d* TMCs over this range, although their identities shift with added exchange to predominantly d^3/d^7 TMCs (i.e., excluding only two Mn(III) and one Cr(II) complex, ESI Table S18). The 4*d* TMCs differ from 3*d* TMCs because most have either an IS (ca. 35%) or LS (ca. 65%) GS, with almost no change in this distribution with a_{HF} value (Figure 8 and ESI Table S18). While all 3*d* metal/oxidation states have at least one GS change from a_{HF} = 0.0 to 0.3, only a small number (i.e., 5 of 45) of d^3 Mo(III) 4*d* TMCs change from LS to IS over this range (Figure 8 and ESI Table S18). This change in GS is somewhat larger than for the Cr(III) TMCs, which are all IS for a_{HF} = 0.2 or above (Figure 8 and ESI Table S18). The d^4 Mo(II) and Tc(III) TMCs favor IS ground states exclusively, whereas most of the 3*d* isovalent Cr(II) or Mn(III) TMCs are HS-favoring especially with increasing a_{HF} values (ESI Table S18). Thus, overall 4*d* TMC GS assignment is significantly less likely to be affected by a change in functional than an equivalent 3*d* TMC although the sensitivity of predicted energies to exchange fraction is only on average reduced by around one third from the first- to second-row TMCs.

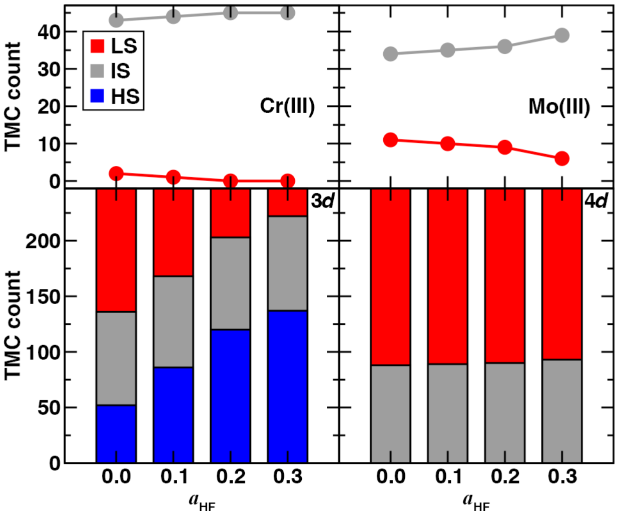

Figure 8. Ground state assignment for the 247 set of 3*d* and 4*d* TMC pairs: LS (red bars and circles), IS (gray bars and circles), and HS (blue bars). (top) Number of 47 pairs that are LS or IS for d^3 Cr(III) (left) or Mo(III) (right) with a_{HF} fraction. (bottom) Stacked bar plot of HS, IS, and LS ground states for all 3*d* (left) and 4*d* (right) TMCs with a_{HF} fraction.

3e. Relationships between energetic sensitivity and structure.

In 3*d* TMCs, increasing spin multiplicity typically leads to longer metal–ligand bond lengths as antibonding states become preferentially occupied over states with bonding character, and this effect is more significant with increasing ligand field. Bond lengths do not change significantly with a_{HF} value[138], and thus structural differences between spin states are also invariant. To determine if structural differences between 3*d* and 4*d* TMC pairs could explain distinct functional sensitivities, we compared the B3LYP structures (i.e., metal–ligand bond lengths) of isovalent complexes. In both 3*d* and 4*d* TMCs, increasing spin multiplicity leads to longer metal–ligand bond lengths, consistent with our expectations, but bond lengths are challenging to directly compare due to the different sizes of 3*d* and 4*d* metals (ESI Figure S3 and Table S20).

As in previous work[138], we facilitate comparison by focusing on relative metal–ligand bond lengths, d_{rel}:

$$d_{\mathrm{rel}}(\text{M-L}) = \frac{d(\text{M-L})}{r_{\mathrm{M}} + r_{\mathrm{L}}} \tag{1}$$

obtained by computing the ratio of the bond length, d, obtained from B3LYP with respect to the substituent metal (M) or ligand (L) atoms' covalent radii, r (ESI Table S20). The d_{rel} values computed and averaged over all six metal–ligand bonds have a similar range of values for both 3d and 4d TMCs (ESI Figure S4 and Tables S21 and S22). For all TMCs, the d_{rel} values increase on average by 0.1 from LS to HS states and increase by about half (ca. 0.05) that amount from LS to IS states (ESI Figure S4 and Tables S21 and S22). The use of an average d_{rel} is a good choice for the fairly symmetric LS states, although some increased asymmetry (e.g., in equatorial vs axial bonds) is apparent in IS or HS states (ESI Figures S5 and S6).

For 3d TMCs, the difference in average relative bond lengths, Δd_{rel}, between HS and LS states is well correlated (R^2 = 0.86) with $S(\Delta E_{\text{H-L}})$ values (Figure 9 and ESI Table S23). The Fe(II)(CO)$_6$ Δd_{rel} is among the largest, consistent with the large magnitude (ca. -175 kcal/mol·HFX) of its $S(\Delta E_{\text{H-L}})$, while Mn(III)(H$_2$O)$_6$ has both a much lower $S(\Delta E_{\text{H-L}})$ (ca. -50 kcal/mol·HFX) and Δd_{rel} of 0.04 (Figure 9). In line with these observations, the overall largest HS-LS Δd_{rel} values are observed for the cases with the most positive $\Delta E_{\text{H-L}}$ values (ESI Figure S7). As with HS-LS, a similar relationship can be observed for $S(\Delta E)$ and Δd_{rel} for the 3d TMC HS-IS or IS-LS splittings (ESI Figure S8 and Table S23). In fact a single good correlation (R^2 = 0.81) can be fit through all three sets of $S(\Delta E)$ and Δd_{rel} values for 3d TMCs (Figure 9 and ESI Figure S8 and Table S23). Taken together with our prior findings[29], these observations suggest that increasing a_{HF} penalizes the delocalized, highly bonded lower-spin states more strongly than higher-spin states. When this bonding difference is larger, the sensitivity to a_{HF} is also higher.

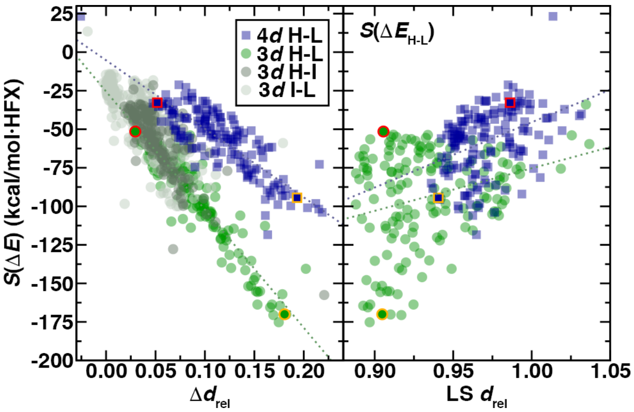

Figure 9. Trends of exchange sensitivity of spin-splitting energies, $S(\Delta E)$ (in kcal/mol·HFX), with averaged relative distance, d_{rel}, quantities: (left) difference in d_{rel} between spin states, Δd_{rel}, and (right) LS d_{rel}. The Δd_{rel} vs $\mathrm{S}(\Delta E)$ trends (left) are shown for 155 pairs of 3*d* TMCs in the case of 4-electron $\Delta E_{\mathrm{H\text{-}L}}$ (green translucent circles), 2-electron $\Delta E_{\mathrm{H\text{-}I}}$ (dark gray translucent circles), and 2-electron $\Delta E_{\mathrm{I\text{-}L}}$ (light gray translucent circles, with an additional 92 I-L only pairs). The results for 4*d* TMCs for the 4-electron $\Delta E_{\mathrm{H\text{-}L}}$ case only are also shown (blue translucent squares). Best-fit lines are shown for all 3*d* (green dotted line) or 4*d* data (blue dotted line). The LS d_{rel} trends vs $S(\Delta E_{\mathrm{H\text{-}L}})$ only are shown at right and follow the same coloring scheme for both symbols and best-fit lines as indicated in left inset legend. For both plots, representative hexa-aqua Mn(III)/Tc(III) HS-LS complex pairs are shown as solid symbols with red outline, and representative hexa-carbonyl Fe(II)/Ru(II) HS-LS complex pairs are shown as solid symbols with orange outline.

For the second-row transition metals, there is also a good correlation ($R^2 = 0.71$) between $S(\Delta E)$ and Δd_{rel} for the HS-LS states of the 4*d* TMCs (Figure 9 and ESI Figure S9 and Table S23). The slope of the relationship however is reduced with respect to values for 3*d* TMCs (Figure 9 and ESI Table S23). Indeed, Δd_{rel} values across all spin-state pairs in 4*d* TMCs are as large as those for the 3*d* TMCs, meaning that differences in Δd_{rel} values cannot be used to explain the reduced exchange sensitivity of 4*d* TMCs (ESI Figure S4). A weaker, but somewhat unified, relationship can be observed between the d_{rel} value of the LS state and $S(\Delta E_{\mathrm{H\text{-}L}})$ across both 3*d* and 4*d* TMCs (Figure 9 and ESI Table S23). Within either 3*d* or 4*d* TMCs, the shortest LS d_{rel} values are observed for the strongest-field (e.g., CO) ligands, which also have the highest exchange sensitivities (Figure 9). Thus, the 4*d* TMCs overlap with some 3*d* TMCs that also have longer LS d_{rel} values (Figure 9 and ESI Figure S4).

To understand the origins of this relationship, we obtained potential energy curves (PECs) over the metal–ligand bond length with varied a_{HF} values for 3*d* and 4*d* TMCs. We contrasted homoleptic helium-atom 3*d*/4*d* complexes as a simplified example of the weak-field limit with strong-field, hexa-carbonyl 3*d*/4*d* TMCs, in which we rigidly displaced the CO ligands (see Sec. 2). In both weak- and strong-field cases, we studied the Ru(II)/Fe(II) complexes in their quintet HS and singlet LS states.

The closed-shell He atoms act as very weak field ligands, with the 3*d*/4*d* TMCs both strongly favoring the HS state over the LS state (B3LYP $\Delta E_{\text{H-L}}$: Fe(II) ca. -64 kcal/mol and Ru(II) ca. -31 kcal/mol, Figure 10 and see ESI Table S24). The $S(\Delta E_{\text{H-L}})$ values are both small and comparable (Fe(II): -47 vs Ru(II): -43 kcal/mol·HFX), consistent with small $S(\Delta E_{\text{H-L}})$ values (hexa-aqua Fe(II): -53 vs Ru(II): -38 kcal/mol·HFX) from other weak-field TMCs (ESI Tables S11 and S24). Despite these comparable exchange sensitivities, the dependence on a_{HF} of individual PECs of Ru(II) and Fe(II) TMCs is distinct (Figure 10). Both HS and LS Ru(II)(He)$_6$ PECs are stabilized with increasing a_{HF}, but the HS relative energy is more sensitive to exchange (Figure 10). For Fe(II)(He)$_6$, on the other hand, the HS PEC is stabilized with increasing a_{HF} while the LS is destabilized (Figure 10). For individual LS or HS states, Ru(II) TMCs PECs have higher sensitivities than the Fe(II) counterparts (Figure 10 and ESI Table S24). The negative $S(\Delta E_{\text{H-L}})$ for Fe(II)(He)$_6$ arises from additive sensitivities of the HS and LS states, while for Ru(II)(He)$_6$ the simultaneous LS and HS stabilization leads to a comparable net $S(\Delta E_{\text{H-L}})$ (Figure 10 and ESI Table S24).

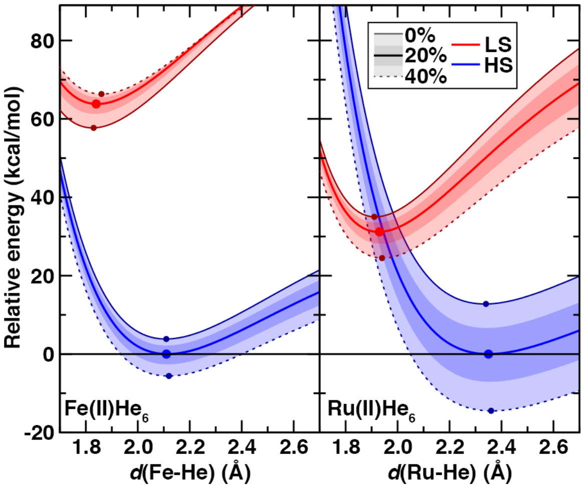

Figure 10. Potential energy curves (PECs, in kcal/mol) with M–He distance (in Å) for Fe(II)(He)$_6$ (left) and Ru(He)$_6$ (right) in LS singlet (red) and HS quintet (blue) spin states. Solid center lines (red for LS and blue for LS, as indicated in inset legend) correspond to the B3LYP (a_{HF} = 0.2) PEC, the outer solid line (maroon for LS and dark blue for HS) corresponds to a_{HF} = 0.0, and the outer dashed line corresponds to a_{HF} = 0.4 (as indicated also in inset legend). The inner shaded regions correspond to the a_{HF} = 0.1-0.3 range, and the outer shaded region to a_{HF} = 0.0-0.4. The relative energies have been aligned to set the minimum of the B3LYP PEC to zero, and a zero line is shown. A circle indicates the minimum of the PECs for a_{HF} = 0.0, 0.2, and 0.4.

The He complexes are weakly bound, with the small covalent radius of the He atom leading to a very long estimated d_{rel} values in LS states for both 3d and 4d TMCs (Fe(II): d_{rel} = 1.08 vs Ru(II): d_{rel} = 1.11) despite moderate absolute bond lengths of 1.84 and 1.93 Å, respectively (Figure 10 and ESI Tables S20 and S24). The HS states are even more weakly bound, leading to large □d_{rel} values of 0.16 for Fe(II) and 0.24 for Ru(II) (Figure 10 and ESI Table S24). Consistent with our expectations, both spin states' d_{rel} and the resulting □d_{rel} are not significantly changed with a_{HF} (Figure 10). Since we can obtain the exchange sensitivity over a wide range of M–He bond lengths in these TMCs, we also evaluated the extent to which S values vary at points away from equilibrium (Figure 10). The vertical HS-LS sensitivity evaluated at the LS geometry for Ru(II) or Fe(II) is comparable to that for the adiabatic case, despite the fact that the LS-HS ordering is inverted at the LS geometry for Ru(II) but unchanged for Fe(II) (Figure 10 and ESI Table S24). When stretched to the HS geometry, the S values decrease significantly for both Ru(II) and Fe(II) (Figure 10 and ESI Table S24).

While the ground state preferences for model strong-field complexes of both Fe(II) and Ru(II) are uniformly LS (B3LYP $\Delta E_{\text{H-L}}$: Fe(II) ca. 30 kcal/mol and Ru(II) ca. 116 kcal/mol), the exchange sensitivity trends are comparable to the weak-field He case (Figure 11 and ESI Table S25). That is, larger total energy sensitivity in the HS Ru(II) PEC still leads to a lower overall $S(\Delta E_{\text{H-L}})$ magnitude compared to Fe(II) because exchange destabilizes the LS 3*d* TMC while weakly stabilizing the LS 4*d* TMC (Figure 11 and ESI Table S25). The only significant distinction observed for the strong-field CO ligands is that *S* for each PEC and the splitting is much more dependent on bond length, with the effect of significantly reducing (>50%) *S* values for vertical spin-state energetics with respect to adiabatic $S(\Delta E_{\text{H-L}})$ values (Figure 11 and ESI Table S25).

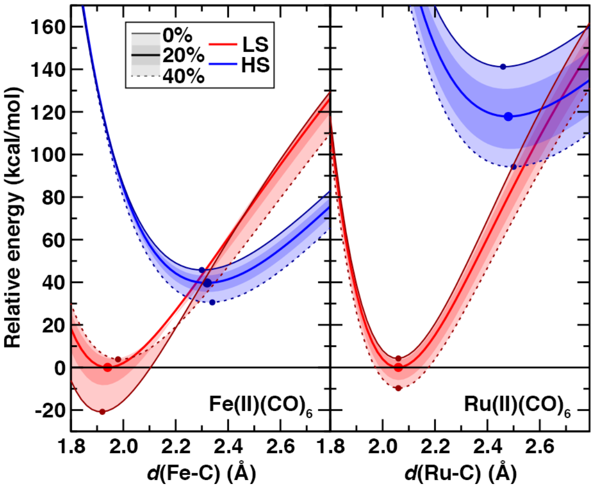

Figure 11. Potential energy curves (PECs, in kcal/mol) with M–C distance (in Å) for Fe(II)(CO)$_6$ (left) and Ru(CO)$_6$ (right) in LS singlet (red) and HS quintet (blue) spin states. Solid center lines (red for LS and blue for LS, as indicated in inset legend) correspond to the B3LYP ($a_{\text{HF}} = 0.2$) PEC, the outer solid line (maroon for LS and dark blue for HS) corresponds to $a_{\text{HF}} = 0.0$, and the outer dashed line corresponds to $a_{\text{HF}} = 0.4$ (as indicated also in inset legend). The inner shaded regions correspond to the $a_{\text{HF}} = 0.1$–0.3 range, and the outer shaded region to $a_{\text{HF}} = 0.0$–0.4. The relative energies have been aligned to set the minimum of the B3LYP PEC to zero, and a zero line is shown. A circle indicates the minimum of the PECs for $a_{\text{HF}} = 0.0$, 0.2, and 0.4.

From the set of all 3*d*/4*d* TMC pairs, over 25 3*d* TMCs have positive sensitivities of the LS total energies whereas only one of the 4*d* TMCs do (ESI Table S26). While average sensitivities of the total energy with respect to a_{HF} are higher for both states in 4*d* TMCs, they are more likely to be similar in magnitude between LS and HS states. Thus, distinct geometric and electronic structure of the LS states of 3*d* TMCs likely contributes to their higher exchange sensitivity (ESI Table S26).

4. Conclusions.

We have carried out a comprehensive study of the extent to which established trends in 3*d* TMC exchange sensitivity and spin-state ordering have analogies in equivalent, isovalent 4*d* TMCs. From ten ligands covering a wide range of ligand field strengths, we generated hundreds of homoleptic and heteroleptic TMCs with a range of mid-row M(II)/M(III) 3*d* and 4*d* metal centers to interpret both 4-electron (i.e., HS-LS) and 2-electron (i.e., HS-IS or IS-LS) spin-splitting energies and sensitivities. We observed consistently increasing exchange sensitivity of $\Delta E_{\text{H-L}}$ with increasing ligand field in both 3*d* and 4*d* TMCs over homoleptic complexes. These observations generalized to representative complexes where strong-field ligand effects were found to be additive in most cases for both $\Delta E_{\text{H-L}}$ and $S(\Delta E_{\text{H-L}})$. Similar trends were observed for HS-IS and IS-LS spin-state energetics, albeit with all magnitudes and ligand-field sensitivities reduced.

The 4*d* TMC exchange sensitivities were consistently smaller in magnitude than the equivalent 3*d* TMC sensitivities for all metals and oxidation states considered. This deviation between 3*d* and 4*d* TMCs increased with increasing ligand-field strength. Despite 4*d* TMC energetics being less sensitive than their 3*d* TMC counterparts, variations by as much as 10 kcal/mol per 10% change in HF exchange were still observed, which could have a significant effect on energetic predictions.

Combined with the significant LS-shifting of 4*d* TMCs with respect to their equivalent 3*d*

TMCs, the reduced 4*d* TMC exchange sensitivity led to a much lower likelihood of change in spin-state ordering than their 3*d* TMC counterparts. While over the range of a_{HF} = 0.0 to 0.3, many 3*d* TMCs changed ground states from LS to IS or HS states, a very small number of 4*d* TMCs shift from LS to IS and none were HS. Analysis of structure confirmed that highly functional-sensitive 3*d* and 4*d* TMCs are characterized by a strong difference between LS and HS metal–ligand bond lengths. Nevertheless, comparison of 3*d* and 4*d* bond length differences between spin states could not explain the reduced sensitivity of 4*d* TMCs, except for a weak correlation of lower sensitivity to the longer LS bond lengths in 4*d* TMCs. Analysis of PECs of representative complexes indicated the higher spin-splitting exchange sensitivities of 3*d* TMCs could be due to the opposing effects of exchange on the two spin states, despite higher exchange-sensitivity of the total energy in 4*d* TMCs.

Overall, we find that while spin-state energetics of 4*d* TMCs are roughly two-thirds as sensitive as those of 3*d* TMCs, this study suggests it is unlikely for HF exchange tuning to alter ground state predictions for 4*d* TMCs. This does not guarantee that common DFT functionals are always capable of predicting the ground state spin but does suggest that conventional tuning approaches that work in 3*d* TMCs to reproduce experimental spin state ordering will not be applicable in 4*d* TMCs.

ASSOCIATED CONTENT

Electronic Supplementary Information is Available Online.

Details of calculation criteria, filtering steps, and eliminated complexes; statistics of sensitivities and relative sensitivities for different spin-splitting energies; sensitivities of pairs of 3*d* and 4*d* TMCs including outliers for different spin splittings; spin splitting and sensitivity properties of CO/H_2O complexes; ground state preference and HS vs LS preference for 3*d* and 4*d* TMCs vs exchange fraction; absolute averaged M-L distances for LS and HS states; covalent radii for computing relative distances; histograms and statistics of relative distances; comparison of equatorial and axial relative distances; relationship between relative distances and exchange sensitivity; properties of potential energy curves for hexa-helium and hexa-carbonyl complexes; and total energy sensitivities of HS and LS states in 239 TMC pairs. (PDF)

Structures and total energies of all 3*d* and 4*d* TMCs studied in this work; reasons complexes or sensitivities were not included in the data set; individual metal-ligand bond lengths for all converged complexes at all exchange fractions; total energy sensitivities in HS-LS pairs of TMCs; individual metal-ligand bond lengths for B3LYP and the relative metal-ligand bond length calculation for all pairs of 3*d*/4*d* TMCs; spin splitting values and sensitivities for all pairs of 3*d*/4*d* TMCs; total energies and analysis of sensitivities for PECs of Fe(II)/Ru(II) homoleptic TMCs in LS and HS states with CO and He atom ligands. (ZIP)

AUTHOR INFORMATION

Corresponding Author

*email: hjkulik@mit.edu phone: 617-253-4584

Notes

The authors declare no competing financial interest.

ACKNOWLEDGMENT

The author acknowledges primary support by the Office of Naval Research under grant number N00014-17-1-2956 (for D.H., N.A., and C.D.) and the National Science Foundation under grant number CBET-1704266 (for A.N.). This work was also supported by the Department of Energy under grant number DE-SC0018096 (for Y.C. and D.B.K.C.). A.N. was partially supported by a National Science Foundation Graduate Research Fellowship under Grant #1122374. This work was carried out in part using computational resources from the Extreme Science and Engineering Discovery Environment (XSEDE), which is supported by National Science Foundation grant number ACI-1548562. H.J.K. holds a Career Award at the Scientific Interface from the Burroughs Wellcome Fund and an AAAS Marion Milligan Mason Award, which supported this work. The authors thank Adam H. Steeves for providing a critical reading of the manuscript.

References

1. Schwarz, H., Ménage-À-Trois: Single-Atom Catalysis, Mass Spectrometry, and Computational Chemistry. *Catalysis Science & Technology* **2017,** *7*, 4302-4314.
2. Schröder, D.; Shaik, S.; Schwarz, H., Two-State Reactivity as a New Concept in Organometallic Chemistry. *Accounts of Chemical Research* **2000,** *33*, 139-145.
3. Shaik, S.; Danovich, D.; Fiedler, A.; Schröder, D.; Schwarz, H., Two-State Reactivity in Organometallic Gas-Phase Ion Chemistry. *Helvetica chimica acta* **1995,** *78*, 1393-1407.
4. Chantarojsiri, T.; Ziller, J. W.; Yang, J. Y., Incorporation of Redox-Inactive Cations Promotes Iron Catalyzed Aerobic C–H Oxidation at Mild Potentials. *Chemical science* **2018,** *9*, 2567-2574.
5. Hoffert, W. A.; Mock, M. T.; Appel, A. M.; Yang, J. Y., Incorporation of Hydrogen-Bonding Functionalities into the Second Coordination Sphere of Iron-Based Water-Oxidation Catalysts. *European Journal of Inorganic Chemistry* **2013,** *2013*, 3846-3857.
6. Foscato, M.; Jensen, V. R., Automated in Silico Design of Homogeneous Catalysts. *ACS Catalysis* **2020,** *10*, 2354-2377.
7. Bousseksou, A.; Molnár, G.; Matouzenko, G., Switching of Molecular Spin States in Inorganic Complexes by Temperature, Pressure, Magnetic Field and Light: Towards Molecular Devices. *European Journal of Inorganic Chemistry* **2004,** *2004*, 4353-4369.
8. Decurtins, S.; Gütlich, P.; Köhler, C.; Spiering, H.; Hauser, A., Light-Induced Excited Spin State Trapping in a Transition-Metal Complex: The Hexa-1-Propyltetrazole-Iron (II) Tetrafluoroborate Spin-Crossover System. *Chemical physics letters* **1984,** *105*, 1-4.
9. Hauser, A., Light-Induced Spin Crossover and the High-Spin→ Low-Spin Relaxation. In *Spin Crossover in Transition Metal Compounds II*, Springer: 2004; pp 155-198.
10. Reed, D. A.; Xiao, D. J.; Gonzalez, M. I.; Darago, L. E.; Herm, Z. R.; Grandjean, F.; Long, J. R., Reversible CO Scavenging via Adsorbate-Dependent Spin State Transitions in an Iron (II)–Triazolate Metal–Organic Framework. *J. Am. Chem. Soc* **2016,** *138*, 5594-5602.
11. Groizard, T.; Papior, N.; Le Guennic, B.; Robert, V.; Kepenekian, M., Enhanced Cooperativity in Supported Spin-Crossover Metal–Organic Frameworks. *The Journal of Physical Chemistry Letters* **2017,** *8*, 3415-3420.
12. Neville, S. M.; Halder, G. J.; Chapman, K. W.; Duriska, M. B.; Moubaraki, B.; Murray, K. S.; Kepert, C. J., Guest Tunable Structure and Spin Crossover Properties in a Nanoporous Coordination Framework Material. *Journal of the American Chemical Society* **2009,** *131*, 12106-12108.
13. Hedström, S.; Chaudhuri, S.; La Porte, N. T.; Rudshteyn, B.; Martinez, J. F.; Wasielewski, M. R.; Batista, V. S., Thousandfold Enhancement of Photoreduction Lifetime in

Re (Bpy)(CO) 3 via Spin-Dependent Electron Transfer from a Perylenediimide Radical Anion Donor. *Journal of the American Chemical Society* **2017,** *139*, 16466-16469.
14. Cramer, C. J.; Truhlar, D. G., Density Functional Theory for Transition Metals and Transition Metal Chemistry. *Physical Chemistry Chemical Physics* **2009,** *11*, 10757-10816.
15. Mori-Sánchez, P.; Cohen, A. J.; Yang, W., Many-Electron Self-Interaction Error in Approximate Density Functionals. *The Journal of chemical physics* **2006,** *125*, 201102.
16. Ruzsinszky, A.; Perdew, J. P.; Csonka, G. I.; Vydrov, O. A.; Scuseria, G. E., Density Functionals That Are One- and Two- Are Not Always Many-Electron Self-Interaction-Free, as Shown for H2+, He2+, LiH+, and Ne2+. *The Journal of Chemical Physics* **2007,** *126*, 104102.
17. Haunschild, R.; Henderson, T. M.; Jiménez-Hoyos, C. A.; Scuseria, G. E., Many-Electron Self-Interaction and Spin Polarization Errors in Local Hybrid Density Functionals. *The Journal of Chemical Physics* **2010,** *133*, 134116.
18. Cohen, A. J.; Mori-Sánchez, P.; Yang, W., Insights into Current Limitations of Density Functional Theory. *Science* **2008,** *321*, 792-794.
19. Schmidt, T.; Kümmel, S., One- and Many-Electron Self-Interaction Error in Local and Global Hybrid Functionals. *Physical Review B* **2016,** *93*, 165120.
20. Kim, M.-C.; Sim, E.; Burke, K., Understanding and Reducing Errors in Density Functional Calculations. *Physical Review Letters* **2013,** *111*, 073003.
21. Zheng, X.; Liu, M.; Johnson, E. R.; Contreras-García, J.; Yang, W., Delocalization Error of Density-Functional Approximations: A Distinct Manifestation in Hydrogen Molecular Chains. *The Journal of Chemical Physics* **2012,** *137*, 214106.
22. Johnson, E. R.; Otero-de-la-Roza, A.; Dale, S. G., Extreme Density-Driven Delocalization Error for a Model Solvated-Electron System. *The Journal of Chemical Physics* **2013,** *139*, 184116.
23. Ruzsinszky, A.; Perdew, J. P.; Csonka, G. I.; Vydrov, O. A.; Scuseria, G. E., Spurious Fractional Charge on Dissociated Atoms: Pervasive and Resilient Self-Interaction Error of Common Density Functionals. *The Journal of chemical physics* **2006,** *125*, 194112.
24. Dutoi, A. D.; Head-Gordon, M., Self-Interaction Error of Local Density Functionals for Alkali–Halide Dissociation. *Chemical Physics Letters* **2006,** *422*, 230-233.
25. Bally, T.; Sastry, G. N., Incorrect Dissociation Behavior of Radical Ions in Density Functional Calculations. *The Journal of Physical Chemistry A* **1997,** *101*, 7923-7925.
26. Zhang, Y.; Yang, W., A Challenge for Density Functionals: Self-Interaction Error Increases for Systems with a Noninteger Number of Electrons. *The Journal of Chemical Physics* **1998,** *109*, 2604-2608.
27. Determan, J. J.; Poole, K.; Scalmani, G.; Frisch, M. J.; Janesko, B. G.; Wilson, A. K., Comparative Study of Nonhybrid Density Functional Approximations for the Prediction of 3d Transition Metal Thermochemistry. *Journal of chemical theory and computation* **2017,** *13*, 4907-4913.
28. Johnson, B. G.; Gonzales, C. A.; Gill, P. M. W.; Pople, J. A., A Density Functional Study of the Simplest Hydrogen Abstraction Reaction. Effect of Self-Interaction Correction. *Chemical Physics Letters* **1994,** *221*, 100-108.
29. Gani, T. Z. H.; Kulik, H. J., Unifying Exchange Sensitivity in Transition Metal Spin-State Ordering and Catalysis through Bond Valence Metrics *Journal of Chemical Theory and Computation* **2017,** *13*, 5443-5457.

30. Gani, T. Z. H.; Kulik, H. J., Where Does the Density Localize? Convergent Behavior for Global Hybrids, Range Separation, and DFT+U *Journal of Chemical Theory and Computation* **2016,** *12*, 5931-5945.
31. Liu, F.; Kulik, H. J., Impact of Approximate DFT Density Delocalization Error on Potential Energy Surfaces in Transition Metal Chemistry. *Journal of Chemical Theory and Computation* **2020,** *16*, 264-277.
32. Srebro, M.; Autschbach, J., Does a Molecule-Specific Density Functional Give an Accurate Electron Density? The Challenging Case of the Cucl Electric Field Gradient. *The Journal of Physical Chemistry Letters* **2012,** *3*, 576-581.
33. Autschbach, J.; Srebro, M., Delocalization Error and “Functional Tuning” in Kohn–Sham Calculations of Molecular Properties. *Accounts of Chemical Research* **2014,** *47*, 2592-2602.
34. Kulik, H. J.; Cococcioni, M.; Scherlis, D. A.; Marzari, N., Density Functional Theory in Transition-Metal Chemistry: A Self-Consistent Hubbard U Approach. *Physical Review Letters* **2006,** *97*, 103001.
35. Ganzenmüller, G.; Berkaïne, N.; Fouqueau, A.; Casida, M. E.; Reiher, M., Comparison of Density Functionals for Differences between the High- (T2g5) and Low- (A1g1) Spin States of Iron(II) Compounds. IV. Results for the Ferrous Complexes [Fe(L)(‘NHS4’)]. *The Journal of Chemical Physics* **2005,** *122*, 234321.
36. Droghetti, A.; Alfè, D.; Sanvito, S., Assessment of Density Functional Theory for Iron (II) Molecules across the Spin-Crossover Transition. *The Journal of chemical physics* **2012,** *137*, 124303.
37. Ioannidis, E. I.; Kulik, H. J., Towards Quantifying the Role of Exact Exchange in Predictions of Transition Metal Complex Properties. *The Journal of Chemical Physics* **2015,** *143*, 034104.
38. Mortensen, S. R.; Kepp, K. P., Spin Propensities of Octahedral Complexes from Density Functional Theory. *The Journal of Physical Chemistry A* **2015,** *119*, 4041-4050.
39. Ioannidis, E. I.; Kulik, H. J., Ligand-Field-Dependent Behavior of Meta-GGA Exchange in Transition-Metal Complex Spin-State Ordering. *The Journal of Physical Chemistry A* **2017,** *121*, 874-884.
40. Liu, F.; Yang, T.; Yang, J.; Xu, E.; Bajaj, A.; Kulik, H. J., Bridging the Homogeneous-Heterogeneous Divide: Modeling Spin and Reactivity in Single Atom Catalysis. *Frontiers in Chemistry* **2019,** *7*, 219.
41. Siig, O. S.; Kepp, K. P., Iron(II) and Iron(III) Spin Crossover: Toward an Optimal Density Functional. *The Journal of Physical Chemistry A* **2018,** *122*, 4208-4217.
42. Phung, Q. M.; Martín-Fernández, C.; Harvey, J. N.; Feldt, M., Ab Initio Calculations for Spin-Gaps of Non-Heme Iron Complexes. *Journal of chemical theory and computation* **2019,** *15*, 4297-4304.
43. Feldt, M.; Phung, Q. M.; Pierloot, K.; Mata, R. A.; Harvey, J. N., Limits of Coupled-Cluster Calculations for Non-Heme Iron Complexes. *Journal of chemical theory and computation* **2019,** *15*, 922-937.
44. Phung, Q. M.; Feldt, M.; Harvey, J. N.; Pierloot, K., Toward Highly Accurate Spin State Energetics in First-Row Transition Metal Complexes: A Combined CASPT2/Cc Approach. *Journal of chemical theory and computation* **2018,** *14*, 2446-2455.
45. Vancoillie, S.; Zhao, H.; Radon, M.; Pierloot, K., Performance of CASPT2 and DFT for Relative Spin-State Energetics of Heme Models. *Journal of chemical theory and computation* **2010,** *6*, 576-582.

46. Nørskov, J. K.; Bligaard, T., The Catalyst Genome. *Angewandte Chemie International Edition* **2013,** *52*, 776-777.
47. Jain, A.; Ong, S. P.; Hautier, G.; Chen, W.; Richards, W. D.; Dacek, S.; Cholia, S.; Gunter, D.; Skinner, D.; Ceder, G.; Persson, K. A., Commentary: The Materials Project: A Materials Genome Approach to Accelerating Materials Innovation. *APL Materials* **2013,** *1*, 011002.
48. KulikGroup molSimplify & molSimplify Automatic Design. https://github.com/hjkgrp/molsimplify (accessed June 1, 2020).
49. Tabor, D. P.; Roch, L. M.; Saikin, S. K.; Kreisbeck, C.; Sheberla, D.; Montoya, J. H.; Dwaraknath, S.; Aykol, M.; Ortiz, C.; Tribukait, H.; Amador-Bedolla, C.; Brabec, C. J.; Maruyama, B.; Persson, K. A.; Aspuru-Guzik, A., Accelerating the Discovery of Materials for Clean Energy in the Era of Smart Automation. *Nature Reviews Materials* **2018,** *3*, 5-20.
50. Curtarolo, S.; Hart, G. L.; Nardelli, M. B.; Mingo, N.; Sanvito, S.; Levy, O., The High-Throughput Highway to Computational Materials Design. *Nature Materials* **2013,** *12*, 191-201.
51. Durand, D. J.; Fey, N., Computational Ligand Descriptors for Catalyst Design. *Chemical reviews* **2019,** *119*, 6561-6594.
52. Gersten, S. W.; Samuels, G. J.; Meyer, T. J., Catalytic Oxidation of Water by an Oxo-Bridged Ruthenium Dimer. *Journal of the American Chemical Society* **1982,** *104*, 4029-4030.
53. Tseng, H.-W.; Zong, R.; Muckerman, J. T.; Thummel, R., Mononuclear Ruthenium (II) Complexes That Catalyze Water Oxidation. *Inorganic chemistry* **2008,** *47*, 11763-11773.
54. Zong, R.; Thummel, R. P., A New Family of Ru Complexes for Water Oxidation. *Journal of the American Chemical Society* **2005,** *127*, 12802-12803.
55. Merki, D.; Hu, X., Recent Developments of Molybdenum and Tungsten Sulfides as Hydrogen Evolution Catalysts. *Energy & Environmental Science* **2011,** *4*, 3878-3888.
56. Zakeeruddin, S.; Nazeeruddin, M. K.; Pechy, P.; Rotzinger, F.; Humphry-Baker, R.; Kalyanasundaram, K.; Grätzel, M.; Shklover, V.; Haibach, T., Molecular Engineering of Photosensitizers for Nanocrystalline Solar Cells: Synthesis and Characterization of Ru Dyes Based on Phosphonated Terpyridines. *Inorganic Chemistry* **1997,** *36*, 5937-5946.
57. Jonas, V.; Thiel, W., Theoretical Study of the Vibrational Spectra of the Transition Metal Carbonyls M (CO) 6 [M= Cr, Mo, W], M (CO) 5 [M= Fe, Ru, Os], and M (CO) 4 [M= Ni, Pd, Pt]. *The Journal of chemical physics* **1995,** *102*, 8474-8484.
58. Waller, M. P.; Braun, H.; Hojdis, N.; Bühl, M., Geometries of Second-Row Transition-Metal Complexes from Density-Functional Theory. *Journal of chemical theory and computation* **2007,** *3*, 2234-2242.
59. Laury, M. L.; Wilson, A. K., Performance of Density Functional Theory for Second Row (4 D) Transition Metal Thermochemistry. *Journal of chemical theory and computation* **2013,** *9*, 3939-3946.
60. Perdew, J. P.; Parr, R. G.; Levy, M.; Balduz, J. L., Density-Functional Theory for Fractional Particle Number: Derivative Discontinuities of the Energy. *Physical Review Letters* **1982,** *49*, 1691-1694.
61. Vydrov, O. A.; Scuseria, G. E.; Perdew, J. P., Tests of Functionals for Systems with Fractional Electron Number. *The Journal of Chemical Physics* **2007,** *126*, 154109.
62. Yang, W.; Zhang, Y.; Ayers, P. W., Degenerate Ground States and a Fractional Number of Electrons in Density and Reduced Density Matrix Functional Theory. *Physical Review Letters* **2000,** *84*, 5172-5175.

63. Perdew, J. P.; Levy, M., Physical Content of the Exact Kohn-Sham Orbital Energies: Band Gaps and Derivative Discontinuities. *Physical Review Letters* **1983,** *51*, 1884-1887.
64. Sham, L. J.; Schlüter, M., Density-Functional Theory of the Energy Gap. *Physical Review Letters* **1983,** *51*, 1888-1891.
65. Sagvolden, E.; Perdew, J. P., Discontinuity of the Exchange-Correlation Potential: Support for Assumptions Used to Find It. *Physical Review A* **2008,** *77*, 012517.
66. Mori-Sanchez, P.; Cohen, A. J., The Derivative Discontinuity of the Exchange-Correlation Functional. *Physical Chemistry Chemical Physics* **2014,** *16*, 14378-14387.
67. Zunger, A.; Freeman, A. J., Ground- and Excited-State Properties of LiF in the Local-Density Formalism. *Physical Review B* **1977,** *16*, 2901-2926.
68. Pederson, M. R.; Heaton, R. A.; Lin, C. C., Density-Functional Theory with Self-Interaction Correction: Application to the Lithium Molecule. *The Journal of Chemical Physics* **1985,** *82*, 2688-2699.
69. Pederson, M. R.; Ruzsinszky, A.; Perdew, J. P., Communication: Self-Interaction Correction with Unitary Invariance in Density Functional Theory. *The Journal of chemical physics* **2014,** *140*, 121103.
70. Kulik, H. J., Perspective: Treating Electron over-Delocalization with the DFT+U Method. *The Journal of Chemical Physics* **2015,** *142*, 240901.
71. Anisimov, V. I.; Zaanen, J.; Andersen, O. K., Band Theory and Mott Insulators - Hubbard-U Instead of Stoner-I. *Physical Review B* **1991,** *44*, 943-954.
72. Liechtenstein, A. I.; Anisimov, V. I.; Zaanen, J., Density-Functional Theory and Strong-Interactions - Orbital Ordering in Mott-Hubbard Insulators. *Physical Review B* **1995,** *52*, R5467-R5470.
73. Dudarev, S. L.; Botton, G. A.; Savrasov, S. Y.; Humphreys, C. J.; Sutton, A. P., Electron-Energy-Loss Spectra and the Structural Stability of Nickel Oxide: An LSDA+U Study. *Physical Review B* **1998,** *57*, 1505-1509.
74. Wilbraham, L.; Adamo, C.; Ciofini, I., Communication: Evaluating Non-Empirical Double Hybrid Functionals for Spin-State Energetics in Transition-Metal Complexes. *The Journal of chemical physics* **2018,** *148*, 041103.
75. Bao, J. L.; Gagliardi, L.; Truhlar, D. G., Self-Interaction Error in Density Functional Theory: An Appraisal. *The journal of physical chemistry letters* **2018,** *9*, 2353-2358.
76. Janesko, B. G., Reducing Density-Driven Error without Exact Exchange. *Physical Chemistry Chemical Physics* **2017,** *19*, 4793-4801.
77. Wilbraham, L.; Verma, P.; Truhlar, D. G.; Gagliardi, L.; Ciofini, I., Multiconfiguration Pair-Density Functional Theory Predicts Spin-State Ordering in Iron Complexes with the Same Accuracy as Complete Active Space Second-Order Perturbation Theory at a Significantly Reduced Computational Cost. *The journal of physical chemistry letters* **2017,** *8*, 2026-2030.
78. Waitt, C.; Ferrara, N. M.; Eshuis, H., Thermochemistry and Geometries for Transition-Metal Chemistry from the Random Phase Approximation. *Journal of chemical theory and computation* **2016,** *12*, 5350-5360.
79. Furche, F.; Perdew, J. P., The Performance of Semilocal and Hybrid Density Functionals in 3d Transition-Metal Chemistry. *The Journal of Chemical Physics* **2006,** *124*, 044103.
80. Zhao, Y.; Truhlar, D. G., The M06 Suite of Density Functionals for Main Group Thermochemistry, Thermochemical Kinetics, Noncovalent Interactions, Excited States, and Transition Elements: Two New Functionals and Systematic Testing of Four M06-Class Functionals and 12 Other Functionals. *Theoretical Chemistry Accounts* **2008,** *120*, 215-241.

81. Swart, M.; Groenhof, A. R.; Ehlers, A. W.; Lammertsma, K., Validation of Exchange−Correlation Functionals for Spin States of Iron Complexes. *The Journal of Physical Chemistry A* **2004,** *108*, 5479-5483.
82. Jensen, K. P.; Cirera, J., Accurate Computed Enthalpies of Spin Crossover in Iron and Cobalt Complexes. *The Journal of Physical Chemistry A* **2009,** *113*, 10033-10039.
83. Ye, S.; Neese, F., Accurate Modeling of Spin-State Energetics in Spin-Crossover Systems with Modern Density Functional Theory. *Inorganic Chemistry* **2010,** *49*, 772-774.
84. Swart, M., Accurate Spin-State Energies for Iron Complexes. *Journal of chemical theory and computation* **2008,** *4*, 2057-2066.
85. Janesko, B. G.; Proynov, E.; Kong, J.; Scalmani, G.; Frisch, M. J., Practical Density Functionals Beyond the Overdelocalization–Underbinding Zero-Sum Game. *The journal of physical chemistry letters* **2017,** *8*, 4314-4318.
86. Stein, T.; Kronik, L.; Baer, R., Prediction of Charge-Transfer Excitations in Coumarin-Based Dyes Using a Range-Separated Functional Tuned from First Principles. *The Journal of Chemical Physics* **2009,** *131*, 244119.
87. Refaely-Abramson, S.; Baer, R.; Kronik, L., Fundamental and Excitation Gaps in Molecules of Relevance for Organic Photovoltaics from an Optimally Tuned Range-Separated Hybrid Functional. *Physical Review B* **2011,** *84*, 075144.
88. Kronik, L.; Stein, T.; Refaely-Abramson, S.; Baer, R., Excitation Gaps of Finite-Sized Systems from Optimally Tuned Range-Separated Hybrid Functionals. *Journal of Chemical Theory and Computation* **2012,** *8*, 1515-1531.
89. Gledhill, J. D.; Peach, M. J. G.; Tozer, D. J., Assessment of Tuning Methods for Enforcing Approximate Energy Linearity in Range-Separated Hybrid Functionals. *Journal of Chemical Theory and Computation* **2013,** *9*, 4414-4420.
90. Karolewski, A.; Kronik, L.; Kümmel, S., Using Optimally Tuned Range Separated Hybrid Functionals in Ground-State Calculations: Consequences and Caveats. *The Journal of Chemical Physics* **2013,** *138*, 204115.
91. Sun, H.; Autschbach, J., Influence of the Delocalization Error and Applicability of Optimal Functional Tuning in Density Functional Calculations of Nonlinear Optical Properties of Organic Donor–Acceptor Chromophores. *ChemPhysChem* **2013,** *14*, 2450-2461.
92. Körzdörfer, T.; Brédas, J.-L., Organic Electronic Materials: Recent Advances in the DFT Description of the Ground and Excited States Using Tuned Range-Separated Hybrid Functionals. *Accounts of Chemical Research* **2014,** *47*, 3284-3291.
93. Leininger, T.; Stoll, H.; Werner, H.-J.; Savin, A., Combining Long-Range Configuration Interaction with Short-Range Density Functionals. *Chemical physics letters* **1997,** *275*, 151-160.
94. Iikura, H.; Tsuneda, T.; Yanai, T.; Hirao, K., A Long-Range Correction Scheme for Generalized-Gradient-Approximation Exchange Functionals. *The Journal of Chemical Physics* **2001,** *115*, 3540-3544.
95. Toulouse, J.; Colonna, F.; Savin, A., Long-Range-Short-Range Separation of the Electron-Electron Interaction in Density-Functional Theory. *Physical Review A* **2004,** *70*, 062505.
96. Baer, R.; Neuhauser, D., Density Functional Theory with Correct Long-Range Asymptotic Behavior. *Physical Review Letters* **2005,** *94*, 043002.
97. Vydrov, O. A.; Scuseria, G. E., Assessment of a Long-Range Corrected Hybrid Functional. *The Journal of Chemical Physics* **2006,** *125*, 234109.

98. Livshits, E.; Baer, R., A Well-Tempered Density Functional Theory of Electrons in Molecules. *Physical Chemistry Chemical Physics* **2007,** *9*, 2932-2941.
99. Cohen, A. J.; Mori-Sánchez, P.; Yang, W., Development of Exchange-Correlation Functionals with Minimal Many-Electron Self-Interaction Error. *The Journal of Chemical Physics* **2007,** *126*, 191109.
100. Salzner, U.; Baer, R., Koopmans' Springs to Life. *The Journal of chemical physics* **2009,** *131*, 231101.
101. Tsuneda, T.; Song, J.-W.; Suzuki, S.; Hirao, K., On Koopmans' Theorem in Density Functional Theory. *The Journal of Chemical Physics* **2010,** *133*, 174101.
102. Mahler, A.; Janesko, B. G.; Moncho, S.; Brothers, E. N., When Hartree-Fock Exchange Admixture Lowers DFT-Predicted Barrier Heights: Natural Bond Orbital Analyses and Implications for Catalysis. *The Journal of chemical physics* **2018,** *148*, 244106.
103. Pritchard, B.; Autschbach, J., Theoretical Investigation of Paramagnetic NMR Shifts in Transition Metal Acetylacetonato Complexes: Analysis of Signs, Magnitudes, and the Role of the Covalency of Ligand–Metal Bonding. *Inorganic chemistry* **2012,** *51*, 8340-8351.
104. Duignan, T.; Autschbach, J., Impact of the Kohn-Sham Delocalization Error on the 4f Shell Localization and Population in Lanthanide Complexes. *Journal of chemical theory and computation* **2016**.
105. Duignan, T.; Autschbach, J.; Batista, E.; Yang, P., Assessment of Tuned Range Separated Exchange Functionals for Spectroscopies and Properties of Uranium Complexes. *Journal of Chemical Theory and Computation* **2017**.
106. Jiang, W.; DeYonker, N. J.; Determan, J. J.; Wilson, A. K., Toward Accurate Theoretical Thermochemistry of First Row Transition Metal Complexes. *The Journal of Physical Chemistry A* **2011,** *116*, 870-885.
107. Moltved, K. A.; Kepp, K. P., The Metal Hydride Problem of Computational Chemistry: Origins and Consequences. *The Journal of Physical Chemistry A* **2019,** *123*, 2888-2900.
108. Bowman, D. N.; Jakubikova, E., Low-Spin Versus High-Spin Ground State in Pseudo-Octahedral Iron Complexes. *Inorganic chemistry* **2012,** *51*, 6011-6019.
109. Smith, D. M.; Dupuis, M.; Straatsma, T., Multiplet Splittings and Other Properties from Density Functional Theory: An Assessment in Iron–Porphyrin Systems. *Molecular Physics* **2005,** *103*, 273-278.
110. Bruschi, M.; De Gioia, L.; Zampella, G.; Reiher, M.; Fantucci, P.; Stein, M., A Theoretical Study of Spin States in Ni-S4 Complexes and Models of the [NiFe] Hydrogenase Active Site. *Journal of Biological Inorganic Chemistry* **2004,** *9*, 873-884.
111. Verma, P.; Varga, Z.; Klein, J. E.; Cramer, C. J.; Que, L.; Truhlar, D. G., Assessment of Electronic Structure Methods for the Determination of the Ground Spin States of Fe (II), Fe (III) and Fe (IV) Complexes. *Physical Chemistry Chemical Physics* **2017,** *19*, 13049-13069.
112. Simm, G. N.; Reiher, M., Systematic Error Estimation for Chemical Reaction Energies. *Journal of chemical theory and computation* **2016,** *12*, 2762-2773.
113. Stein, T.; Autschbach, J.; Govind, N.; Kronik, L.; Baer, R., Curvature and Frontier Orbital Energies in Density Functional Theory. *The journal of physical chemistry letters* **2012,** *3*, 3740-3744.
114. Skone, J. H.; Govoni, M.; Galli, G., Self-Consistent Hybrid Functional for Condensed Systems. *Physical Review B* **2014,** *89*, 195112.

115. Shimazaki, T.; Asai, Y., First Principles Band Structure Calculations Based on Self-Consistent Screened Hartree–Fock Exchange Potential. *The Journal of chemical physics* **2009,** *130*, 164702.

116. Ashley, D. C.; Jakubikova, E., Ironing out the Photochemical and Spin-Crossover Behavior of Fe(II) Coordination Compounds with Computational Chemistry. *Coordination Chemistry Reviews* **2017,** *337*, 97-111.

117. Reiher, M., Theoretical Study of the Fe (Phen) 2 (NCS) 2 Spin-Crossover Complex with Reparametrized Density Functionals. *Inorganic Chemistry* **2002,** *41*, 6928-6935.

118. Bleda, E. A.; Trindle, C.; Altun, Z., Studies on Spin State Preferences in Fe(II) Complexes. *Computational and Theoretical Chemistry* **2015,** *1073*, 139-148.

119. Janet, J. P.; Chan, L.; Kulik, H. J., Accelerating Chemical Discovery with Machine Learning: Simulated Evolution of Spin Crossover Complexes with an Artificial Neural Network. *The Journal of Physical Chemistry Letters* **2018,** *9*, 1064-1071.

120. Burke, K., Perspective on Density Functional Theory. *The Journal of chemical physics* **2012,** *136*, 150901.

121. Becke, A. D., Perspective: Fifty Years of Density-Functional Theory in Chemical Physics. *The Journal of chemical physics* **2014,** *140*, 18A301.

122. Janet, J. P.; Zhao, Q.; Ioannidis, E. I.; Kulik, H. J., Density Functional Theory for Modelling Large Molecular Adsorbate-Surface Interactions: A Mini-Review and Worked Example. *Mol Simulat* **2017,** *43*, 327-345.

123. Deeth, R. J.; Fey, N., The Performance of Nonhybrid Density Functionals for Calculating the Structures and Spin States of Fe (II) and Fe (III) Complexes. *Journal of computational chemistry* **2004,** *25*, 1840-1848.

124. Coskun, D.; Jerome, S. V.; Friesner, R. A., Evaluation of the Performance of the B3LYP, PBE0, and M06 DFT Functionals, and DBLOC-Corrected Versions, in the Calculation of Redox Potentials and Spin Splittings for Transition Metal Containing Systems. *Journal of chemical theory and computation* **2016,** *12*, 1121-1128.

125. Hughes, T. F.; Friesner, R. A., Correcting Systematic Errors in DFT Spin-Splitting Energetics for Transition Metal Complexes. *Journal of chemical theory and computation* **2011,** *7*, 19-32.

126. Kepp, K. P., Theoretical Study of Spin Crossover in 30 Iron Complexes. *Inorganic Chemistry* **2016,** *55*, 2717-2727.

127. Zein, S.; Borshch, S. A.; Fleurat-Lessard, P.; Casida, M. E.; Chermette, H., Assessment of the Exchange-Correlation Functionals for the Physical Description of Spin Transition Phenomena by Density Functional Theory Methods: All the Same? *The Journal of Chemical Physics* **2007,** *126*, 014105.

128. Boguslawski, K.; Jacob, C. R.; Reiher, M., Can DFT Accurately Predict Spin Densities? Analysis of Discrepancies in Iron Nitrosyl Complexes. *Journal of Chemical Theory and Computation* **2011,** *7*, 2740-2752.

129. Milko, P.; Iron, M. A., On the Innocence of Bipyridine Ligands: How Well Do DFT Functionals Fare for These Challenging Spin Systems? *Journal of Chemical Theory and Computation* **2014,** *10*, 220-235.

130. Sproviero, E. M.; Gascon, J. A.; McEvoy, J. P.; Brudvig, G. W.; Batista, V. S., Characterization of Synthetic Oxomanganese Complexes and the Inorganic Core of the O2-Evolving Complex in Photosystem II: Evaluation of the DFT/B3LYP Level of Theory. *Journal of inorganic biochemistry* **2006,** *100*, 786-800.

131. Reiher, M.; Salomon, O.; Hess, B. A., Reparameterization of Hybrid Functionals Based on Energy Differences of States of Different Multiplicity. *Theoretical Chemistry Accounts* **2001,** *107*, 48-55.
132. Salomon, O.; Reiher, M.; Hess, B. A., Assertion and Validation of the Performance of the B3LYP* Functional for the First Transition Metal Row and the G2 Test Set. *Journal of Chemical Physics* **2002,** *117*, 4729-4737.
133. Fouqueau, A.; Mer, S.; Casida, M. E.; Lawson Daku, L. M.; Hauser, A.; Mineva, T.; Neese, F., Comparison of Density Functionals for Energy and Structural Differences between the High- [5t2g:(T2g)4(Eg)2] and Low- [1a1g:(T2g)6(Eg)0] Spin States of the Hexaquoferrous Cation [Fe(H2O)6]2+. *The Journal of Chemical Physics* **2004,** *120*, 9473-9486.
134. Fouqueau, A.; Casida, M. E.; Lawson Daku, L. M.; Hauser, A.; Neese, F., Comparison of Density Functionals for Energy and Structural Differences between the High-[5t2g:(T2g) 4 (Eg) 2] and Low-[1a1g:(T2g) 6 (Eg) 0] Spin States of Iron (II) Coordination Compounds. II. More Functionals and the Hexaminoferrous Cation,[Fe (NH3) 6] 2+. *The Journal of Chemical Physics* **2005,** *122*, 044110.
135. Adamo, C.; Barone, V., Toward Reliable Density Functional Methods without Adjustable Parameters: The PBE0 Model. *The Journal of chemical physics* **1999,** *110*, 6158-6170.
136. Janet, J. P.; Kulik, H. J., Predicting Electronic Structure Properties of Transition Metal Complexes with Neural Networks. *Chemical Science* **2017,** *8*, 5137-5152.
137. Kulik, H. J., Making Machine Learning a Useful Tool in the Accelerated Discovery of Transition Metal Complexes. *Wiley Interdisciplinary Reviews: Computational Molecular Science* **2020,** *10*, e1439.
138. Taylor, M. G.; Yang, T.; Lin, S.; Nandy, A.; Janet, J. P.; Duan, C.; Kulik, H. J., Seeing Is Believing: Experimental Spin States from Machine Learning Model Structure Predictions. *The Journal of Physical Chemistry A* **2020,** *124*, 3286-3299.
139. Janet, J. P.; Liu, F.; Nandy, A.; Duan, C.; Yang, T.; Lin, S.; Kulik, H. J., Designing in the Face of Uncertainty: Exploiting Electronic Structure and Machine Learning Models for Discovery in Inorganic Chemistry. *Inorganic Chemistry* **2019,** *58*, 10592-10606.
140. Tsuchida, R., Absorption Spectra of Co-ordination Compounds. I. *BCSJ* **1938,** *13*, 388-400.
141. Nandy, A.; Duan, C.; Janet, J. P.; Gugler, S.; Kulik, H. J., Strategies and Software for Machine Learning Accelerated Discovery in Transition Metal Chemistry. *Industrial & Engineering Chemistry Research* **2018,** *57*, 13973-13986.
142. Duan, C.; Janet, J. P.; Liu, F.; Nandy, A.; Kulik, H. J., Learning from Failure: Predicting Electronic Structure Calculation Outcomes with Machine Learning Models. *Journal of Chemical Theory and Computation* **2019,** *15*, 2331-2345.
143. Ioannidis, E. I.; Gani, T. Z. H.; Kulik, H. J., molSimplify: A Toolkit for Automating Discovery in Inorganic Chemistry. *J. Comput. Chem.* **2016,** *37*, 2106-2117.
144. KulikGroup molSimplify Documentation. http://molsimplify.mit.edu (accessed June 1, 2020).
145. O'Boyle, N. M.; Banck, M.; James, C. A.; Morley, C.; Vandermeersch, T.; Hutchison, G. R., Open Babel: An Open Chemical Toolbox. *J Cheminform* **2011,** *3*, 33.
146. O'Boyle, N. M.; Morley, C.; Hutchison, G. R., Pybel: A Python Wrapper for the Openbabel Cheminformatics Toolkit. *Chem Cent J* **2008,** *2*, 5.

147. Ufimtsev, I. S.; Martinez, T. J., Quantum Chemistry on Graphical Processing Units. 3. Analytical Energy Gradients, Geometry Optimization, and First Principles Molecular Dynamics. *Journal of Chemical Theory and Computation* **2009,** *5*, 2619-2628.
148. Petachem. http://www.petachem.com. (accessed June 1, 2020).
149. Becke, A. D., Density-Functional Thermochemistry. III. The Role of Exact Exchange. *Journal of Chemical Physics* **1993,** *98*, 5648-5652.
150. Lee, C.; Yang, W.; Parr, R. G., Development of the Colle-Salvetti Correlation-Energy Formula into a Functional of the Electron Density. *Physical Review B* **1988,** *37*, 785--789.
151. Stephens, P. J.; Devlin, F. J.; Chabalowski, C. F.; Frisch, M. J., Ab Initio Calculation of Vibrational Absorption and Circular Dichroism Spectra Using Density Functional Force Fields. *The Journal of Physical Chemistry* **1994,** *98*, 11623-11627.
152. Hay, P. J.; Wadt, W. R., Ab Initio Effective Core Potentials for Molecular Calculations. Potentials for the Transition Metal Atoms Sc to Hg. *Journal of Chemical Physics* **1985,** *82*, 270-283.
153. Saunders, V. R. H., I. H., A "Level-Shifting" Method for Converging Closed Shell Hartree-Fock Wave Functions. *Int J Quantum Chem* **1973,** *7*, 699-705.
154. Wang, L.-P.; Song, C., Geometry Optimization Made Simple with Translation and Rotation Coordinates. *The Journal of Chemical Physics* **2016,** *144*, 214108.
155. Janet, J. P.; Duan, C.; Yang, T.; Nandy, A.; Kulik, H. J., A Quantitative Uncertainty Metric Controls Error in Neural Network-Driven Chemical Discovery. *Chemical Science* **2019,** *10*, 7913-7922.
156. Zhao, Q.; Kulik, H. J., Stable Surfaces That Bind Too Tightly: Can Range Separated Hybrids or DFT+U Improve Paradoxical Descriptions of Surface Chemistry? *The Journal of Physical Chemistry Letters* **2019,** *10*, 5090-5098.
157. Zhao, Q.; Kulik, H. J., Where Does the Density Localize in the Solid State? Divergent Behavior for Hybrids and DFT+U. *Journal of Chemical Theory and Computation* **2018,** *14*, 670-683.
158. Gütlich, P., Spin Crossover in Iron (II)-Complexes. In *Metal Complexes*, Springer: 1981; pp 83-195.